NUREG/CR-6875
ANL-04/08

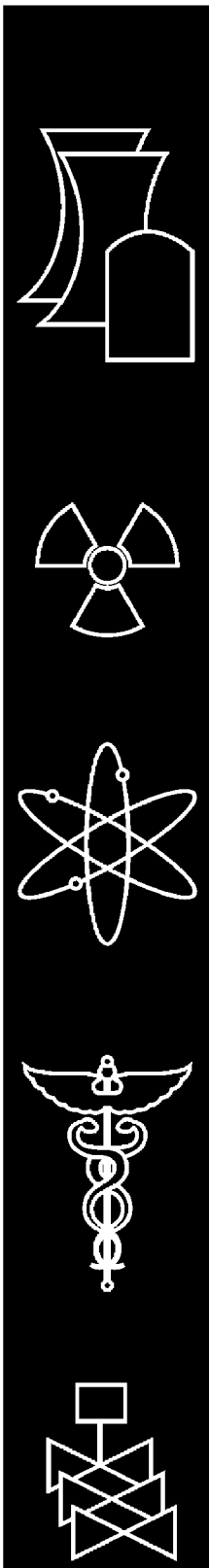

Boric Acid Corrosion of Light Water Reactor Pressure Vessel Materials

Argonne National Laboratory

U.S. Nuclear Regulatory Commission
Office of Nuclear Regulatory Research
Washington, DC 20555-0001

AVAILABILITY OF REFERENCE MATERIALS IN NRC PUBLICATIONS

NRC Reference Material

As of November 1999, you may electronically access NUREG-series publications and other NRC records at NRC's Public Electronic Reading Room at http://www.nrc.gov/reading-rm.html. Publicly released records include, to name a few, NUREG-series publications; *Federal Register* notices; applicant, licensee, and vendor documents and correspondence; NRC correspondence and internal memoranda; bulletins and information notices; inspection and investigative reports; licensee event reports; and Commission papers and their attachments.

NRC publications in the NUREG series, NRC regulations, and *Title 10, Energy*, in the Code of *Federal Regulations* may also be purchased from one of these two sources.

1. The Superintendent of Documents
   U.S. Government Printing Office
   Mail Stop SSOP
   Washington, DC 20402–0001
   Internet: bookstore.gpo.gov
   Telephone: 202-512-1800
   Fax: 202-512-2250
2. The National Technical Information Service
   Springfield, VA 22161–0002
   www.ntis.gov
   1–800–553–6847 or, locally, 703–605–6000

A single copy of each NRC draft report for comment is available free, to the extent of supply, upon written request as follows:

Address: Office of the Chief Information Officer,
Reproduction and Distribution
Services Section
U.S. Nuclear Regulatory Commission
Washington, DC 20555-0001
E-mail: DISTRIBUTION@nrc.gov
Facsimile: 301–415–2289

Some publications in the NUREG series that are posted at NRC's Web site address http://www.nrc.gov/reading-rm/doc-collections/nuregs are updated periodically and may differ from the last printed version. Although references to material found on a Web site bear the date the material was accessed, the material available on the date cited may subsequently be removed from the site.

Non-NRC Reference Material

Documents available from public and special technical libraries include all open literature items, such as books, journal articles, and transactions, *Federal Register* notices, Federal and State legislation, and congressional reports. Such documents as theses, dissertations, foreign reports and translations, and non-NRC conference proceedings may be purchased from their sponsoring organization.

Copies of industry codes and standards used in a substantive manner in the NRC regulatory process are maintained at—

The NRC Technical Library
Two White Flint North
11545 Rockville Pike
Rockville, MD 20852–2738

These standards are available in the library for reference use by the public. Codes and standards are usually copyrighted and may be purchased from the originating organization or, if they are American National Standards, from—

American National Standards Institute
11 West 42nd Street
New York, NY 10036–8002
www.ansi.org
212–642–4900

Legally binding regulatory requirements are stated only in laws; NRC regulations; licenses, including technical specifications; or orders, not in NUREG-series publications. The views expressed in contractor-prepared publications in this series are not necessarily those of the NRC.

The NUREG series comprises (1) technical and administrative reports and books prepared by the staff (NUREG–XXXX) or agency contractors (NUREG/CR–XXXX), (2) proceedings of conferences (NUREG/CP–XXXX), (3) reports resulting from international agreements (NUREG/IA–XXXX), (4) brochures (NUREG/BR–XXXX), and (5) compilations of legal decisions and orders of the Commission and Atomic and Safety Licensing Boards and of Directors' decisions under Section 2.206 of NRC's regulations (NUREG–0750).

NUREG/CR-6875
ANL-04/08

Boric Acid Corrosion of Light Water Reactor Pressure Vessel Materials

Manuscript Completed: May 2004
Date Published: July 2005

Prepared by
J.-H. Park, O. K. Chopra, K. Natesan, and W. J. Shack

Energy Technology Division
Argonne National Laboratory
9700 South Cass Avenue
Argonne, IL 60439

W. H. Cullen, Jr., NRC Project Manager

Prepared for
Division of Engineering Technology
Office of Nuclear Regulatory Research
U.S. Nuclear Regulatory Commission
Washington, DC 20555-0001
NRC Job Code Y6722

Abstract

This report presents experimental data on electrochemical potential and corrosion rates of the materials found in the reactor pressure vessel head and control rod drive mechanism (CRDM) nozzles in boric acid solutions of varying concentrations at temperatures of 95–316°C (203–600°F). Tests were conducted in (a) high–temperature, high–pressure aqueous solutions with a range of boric acid concentrations, (b) high-temperature (150–316°C) H-B-O solutions at ambient pressure, wetted and dry, and (c) low–temperature (≈95°C) saturated, aqueous, boric acid solutions. These correspond to the following situations: (a) low leakage through the nozzle and nozzle/head annulus plugged, (b) low leakage through the nozzle and nozzle/head annulus open, and (c) significant cooling due to high leakage and nozzle/head annulus open. The results indicate significant corrosion only for the low–alloy steel and no corrosion for Alloy 600 or 308 stainless steel cladding. Also, corrosion rates were significant in saturated boric acid solutions, and no material loss was observed in boric acid melts or deposits in the absence of moisture. The results are compared with the existing corrosion/wastage data in the literature.

Foreword

In the aftermath of the discovery of a corrosion cavity in the vessel head at the Davis-Besse Nuclear Power Station in March 2002, the U.S. Nuclear Regulatory Commission (NRC) renewed its effort to understand the mechanics and chemistry that occur during the corrosion process. Based on the results of corrosion testing over the preceding 15 or so years, the prevailing thinking at that time was that corrosion in an aqueous-based solution could not occur at an elevated temperature, because water would evaporate and dry boric acid salts were "known" to be non-corrosive. However, such thinking did not account for the corrosion rates that had prevailed on the Davis-Besse reactor head. Against that background, the NRC's Office of Nuclear Regulatory Research, together with Argonne National Laboratory, completed a test program to determine the corrosion rates of important reactor structural materials over a wide range of temperatures and boric acid solution concentrations. This report presents the resultant corrosion rate and electrochemical potential data.

As part of the investigation of the Davis-Besse reactor head corrosion event, industry analysts developed a model that suggested that the evaporative cooling effect would reduce the temperature of the pool of accumulating liquid to about 93 °C (200 °F) as the leak rate approached and exceeded about 0.4 liter (0.1 gallon) per minute. This finding is important because this temperature is significantly cooler than assumed in earlier testing and does not support the thinking that an aqueous-based boric acid solution would not exist because the water would evaporate. This report contains data showing that corrosion rates of low-alloy steel at that temperature are a strong function of solution concentration, and reach about 100 mm (3.9 inches) per year in saturated solutions. Further, this report describes, for the first time, tests in slightly wetted boric acid salts at temperatures of 150 °C (302 °F) and 170 °C (338 °F). The data from these tests show that corrosion rates of low-alloy steel in this mixture can actually exceed those of aqueous solutions, reaching 125 mm (4.9 inches) to 150 mm (5.9 inches) per year at 150 °C (302 °F).

On a positive note, this report contains data showing that stainless steel cladding materials and Alloy 600 do not corrode significantly in any combination of temperature and solution concentration tested within the scope of this program. Likewise, the electrochemical potential (ECP) values for the materials and solutions tested in this program support the conclusion that ECP differences among the relevant combinations of structural materials are too small to give rise to the possibility of any significant galvanic reactions.

The data derived from this study will expand the existing database of corrosion rates for reactor structural materials in boric acid solutions, and much of the data will be included in the Boric Acid Corrosion Guidebook (Reference 5). Nonetheless, when applying any conclusions based on these data, users should remain within the bounds of the tested parameters; extrapolation of these results could lead to erroneous conclusions. Users should also be aware that composition differences among reactor and low-carbon steels could result in inaccurate estimates of corrosion rates for materials that were not actually tested in this program.

Carl J. Paperiello, Director
Office of Nuclear Regulatory Research
U.S. Nuclear Regulatory Commission

Contents

Figures

Tables

Executive Summary

In March 2002, during inspections at the Davis-Besse (D-B) nuclear power station in response to NRC Bulletin 2001-01, axial cracks were identified in five control rod drive mechanism (CRDM) nozzles near the J–groove weld. Also, significant degradation of the reactor pressure vessel (RPV) head base metal was discovered downhill of nozzle #3; a triangular cavity, ≈127 mm (5 in.) width and 178 mm (7 in.) long and completely through the low-alloy steel RPV head thickness (≈178 mm), had been created. Although cracking of Alloy 600 CRDM nozzles by primary water stress corrosion cracking (PWSCC) is a known degradation mechanism and has been observed at other nuclear power plants, damage of this magnitude to the RPV head caused by boric acid corrosion had not been anticipated. In the other instances of CRDM nozzle cracking, total leakage from the crack into the annulus appears to have been very low and occurred at very low leakage rates. At low leak rates (≈10^{-6} to 10^{-5} gpm), the leaking flow completely vaporizes to steam immediately downstream from the principal flashing location resulting in a dry annulus and no loss of material. The D-B experience demonstrates that this is not always the case.

It is important to understand the conditions that can result in this aggressive attack. The critical issue is why the leaking nozzle #3 at D-B progressed to high leak rates and significant RPV head wastage. Corrosion/wastage of RPV steel in concentrated boric acid solutions is not well described or quantified in the literature, and especially not under the temperature, flow, and concentration of species that may have occurred on the D-B head. The electrochemical potentials (ECPs) of the alloys in the aqueous solutions involved are also not known.

This report presents experimental data on ECP and corrosion/wastage rates of the materials found in the RPV head and nozzles of the D–B reactor in boric acid solutions of varying concentrations at temperatures of 95–316°C (203–600°F). Tests were conducted in environmental conditions that have been postulated in the CRDM nozzle/head crevice: (i) high–temperature, high–pressure aqueous environment with a range of boric acid solution concentrations; (ii) high-temperature (150–300°C) boric acid powder at atmospheric pressure with and without the addition of water; and (iii) low–temperature (≈95°C) saturated boric acid solution both deaerated and aerated. These environmental conditions correspond to the following situations: (a) low leakage through nozzle crack and nozzle/head annulus plugged, (b) low leakage through nozzle crack and nozzle/head annulus open, and (c) significant cooling due to high leakage through nozzle crack and nozzle/head annulus open.

Test facilities were assembled to perform ECP and corrosion rate measurements on A533 Gr.–B low–alloy steel, Alloy 600, and 308 SS weld clad, in the various postulated environments in the CRDM nozzle/head crevice. In general, the ECP of all alloys decreased with an increase in temperature. At temperatures below 150°C the ECP of A533 Gr.–B low–alloy steel was significantly lower than that of the other alloys. Also, at 95°C, the ECP of A533 Gr.–B steel decreased slightly as the concentration of boric acid in the solution was decreased from 36,000 ppm to 3,500 ppm. At 150–316°C and 12.4 MPa (1800 psi) pressure, the ECP of all alloys are comparable in water with 1000 or 9090 ppm B, ≈2 ppm Li, <10 ppb dissolved oxygen (DO), and ≈2 ppm dissolved hydrogen.

In the various environments investigated in the present study, the corrosion rates of Alloy 600 and 308 SS cladding were found to be negligible compared to those of A533 Gr.–B

steel. Also, in the absence of moisture, no corrosion was observed for any of the materials in H–B–O environments at 150, 260, and 300°C; the H–B–O environments consist of a dry powder of HBO_2 + H_3BO_3 at 150°C, molten HBO_2 at 260°C, and molten mixture of HBO_2 + B_2O_3 at 300°C.

For A533 Gr.–B steel, an average corrosion rate of ≈40 mm/y (1.6 in./y) was measured in aerated saturated solution of boric acid at 97.5°C and ambient pressure. The corrosion rate in aerated half–saturated solution was a factor of ≈2 lower than in saturated solution; the rates for deaerated solution were ≈40% lower than in aerated solution. Very high corrosion rates were observed for A533 Gr.–B steel at 140–170°C in molten salt solutions of boric acid with addition of water. Corrosion rates up to 150 mm/y were measured at 150°C.

The corrosion experiments in high–temperature high–pressure water containing 9090 ppm B, ≈2 ppm Li, <10 ppb DO, and ≈2 ppm dissolved hydrogen showed that the corrosion rates decreased with increasing temperature. The rates were ≈5 mm/y at 100–150°C and decreased to <0.1 mm/y at 316°C.

The existing corrosion/wastage data in the literature have been summarized. The results from the present study have been compared with the available data to assess the corrosion performance of the RPV and CRDM nozzle materials in boric acid solutions.

Abbreviations

ANL	Argonne National Laboratory
ASTM	American Society for Testing and Materials
BNL	Brookhaven National Laboratory
CGR	Crack growth rate
CR	Corrosion rate
CRDM	Control rod drive mechanism
D-B	Davis Besse
DO	Dissolved oxygen
ECP	Electrochemical potential
EDX	Energy dispersive x–ray spectroscopy
EPRI	Electric Power Research Institute
ID	Inner diameter
NDE	nondestructive examination
NRC	Nuclear Regulatory Commission
OD	Outer diameter
PWR	Pressurized water reactor
PWSCC	Primary water stress corrosion cracking
RCS	Reactor coolant system
RPV	Reactor pressure vessel
RT	Room temperature
SCE	Saturated calomel electrode
SEM	Scanning electron microscopy
SHE	Standard hydrogen electrode

SMA	Shielded metal arc
SS	Stainless steel
TGA	Thermogravimetric analysis
UHP	Ultra high purity
WE	Working electrode
wppm	parts per million by weight

Acknowledgments

The authors thank R. W. Clark and E. J. Listwan for their contributions to the experimental effort. This work is sponsored by the Office of Nuclear Regulatory Research, U.S. Nuclear Regulatory Commission, Job Code Y6722; Program Manager: W. H. Cullen, Jr.

1. Introduction

In early March 2002, during inspections at the Davis-Besse (D-B) nuclear power station in response to NRC Bulletin 2001-01,[1] boric acid crystal deposits and iron oxide were observed at several openings in the lower service structure support skirt. Follow–up non–destructive examination (NDE) identified axial cracks in five control rod drive mechanism (CRDM) nozzles near the J–groove weld.[2] These cracks had initiated from the inner diameter (ID) of the nozzle and were attributed to primary water stress corrosion cracking (PWSCC). Three of these CRDM nozzles (#1, #2, and #3), located near the center of the reactor pressure vessel (RPV) head, contained through–wall cracks. In addition to the axial cracks CRDM nozzle #2 contained a circumferential crack that had initiated from the outer diameter (OD) of the nozzle.

Repair of these five CRDM nozzles required boring out the lower portion of the CRDM nozzle containing the cracks and the J–groove weld, and re–welding the remaining nozzles back to the RPV head. However, after boring out the lower portion of CRDM nozzle #3, significant degradation of the RPV head base metal was discovered between nozzles #3 and #11. Downhill of nozzle #3, a roughly triangular cavity, ≈127 mm (5 in.) width and 178 mm (7 in.) long and completely through the low-alloy steel RPV head thickness (≈178 mm), had been created.[2,3] A schematic diagram of the D–B RPV head showing the area of RPV head degradation is presented in Fig. 1. A schematic drawing and photograph of the overhead view of the corrosion cavity are shown in Fig. 2. Between 650 and 980 cc (40 and 60 in.^{3}) of metal had corroded and been flushed from the cavity, leaving only a layer of cladding about 7.6 mm (0.3 in.) thick, with an exposed surface area of 130–160 cm^2 (21–25 in.^{2}). Some minor corrosion degradation was also observed in CRDM nozzle #2.[3]

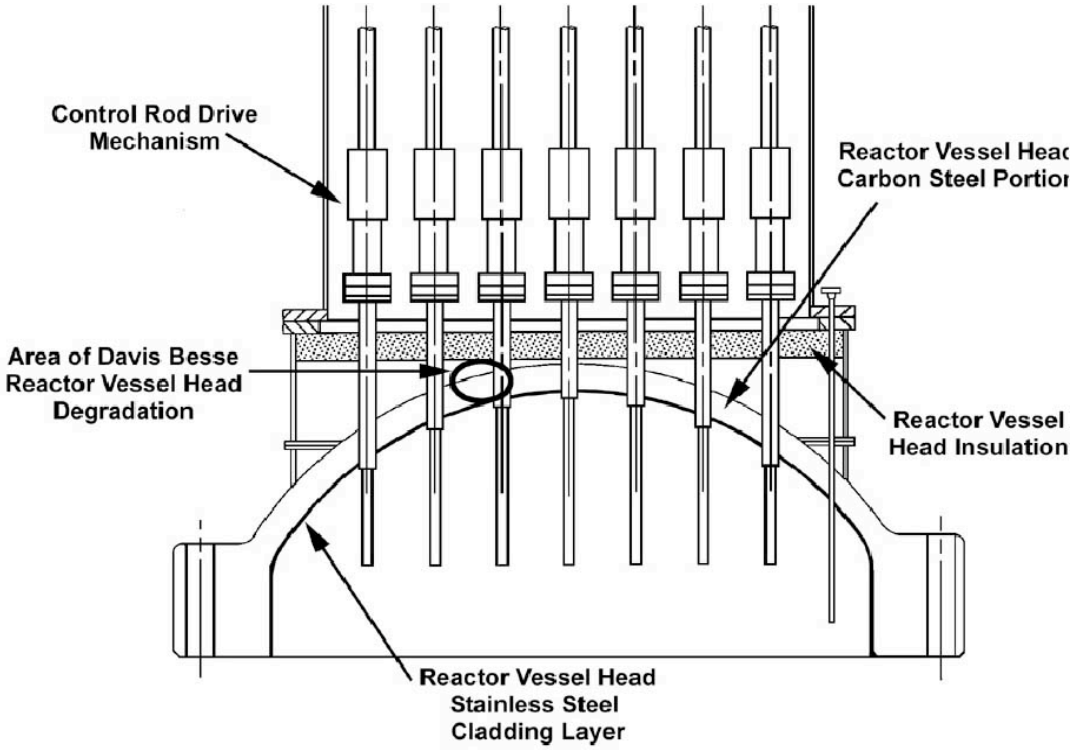

Figure 1. Reactor pressure vessel head at the Davis-Besse nuclear generating station.

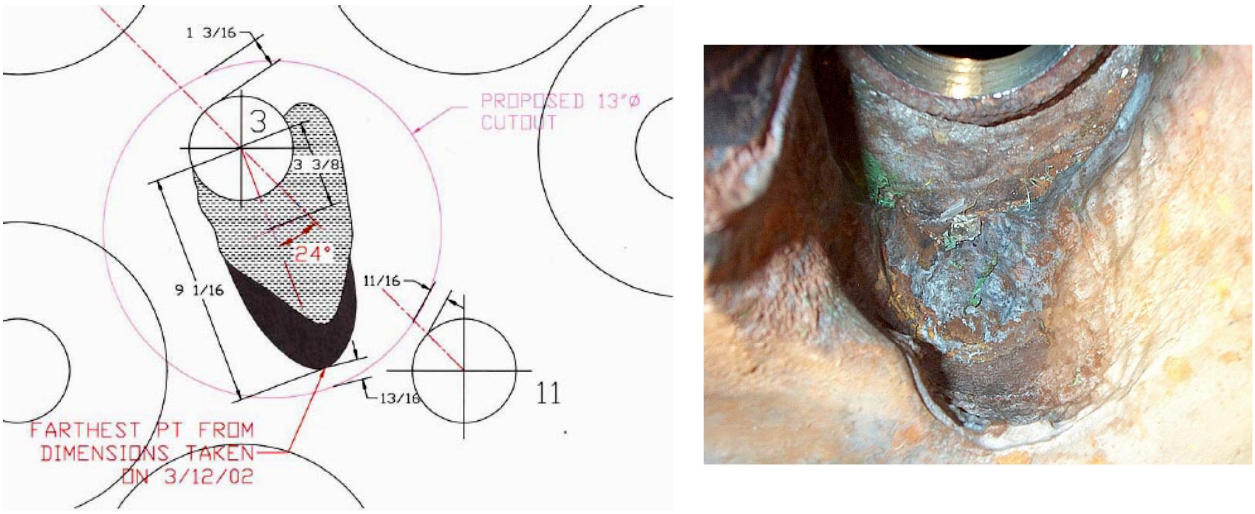

Figure 2. Severe corrosion on the exterior surface of the RPV head between CRDM nozzle #3 and nozzle #11 at the Davis-Besse nuclear power station.

Although PWSCC of Alloy 600 CRDM nozzles is a known degradation mechanism and has been observed at other nuclear power plants,[4] damage of this magnitude to the RPV head had not been anticipated. In the other instances of throughwall cracking of CRDM nozzles, total leakage from the crack into the annulus appears to have been very low and occurred at very low leakage rates. The D-B experience demonstrates that this is not always the case. It is important to understand the conditions that can result in this aggressive attack. The critical issue is why the leaking nozzle #3 at D-B progressed to high leak rates and significant RPV head wastage.

After discovery of the cavity, a root cause report[3] was issued describing the background and events leading up to the discovery, together with a host of "contributing causes" that resulted in the CRDM leaks and the ensuing RPV head corrosion. The root cause report suggests a scenario for the degradation of RPV head base metal:

(a) Crack initiation and growth to throughwall. The report postulates that a crack initiated in nozzle #3 in about 1990 (≈3 years after plant operation began) due to PWSCC. The crack grew to a throughwall crack that penetrated above the J-groove weld in 1994 to 1996. The report hypothesizes that at this stage, the extent of throughwall cracking was very limited and that leakage from the reactor coolant system (RCS) would have been extremely small.

(b) *Minor weepage/latency period.* As the crack grew, RCS leakage would have entered the annular region between the Alloy 600 nozzle and low-alloy steel RPV head. A schematic diagram of the D–B CRDM nozzle is shown in Fig. 3. With addition of moist boric acid from the newly developed crack into the bimetallic annulus, various corrosion and concentration processes (including galvanic attack) would have become possible. The report proposes that these corrosion processes would open the annular gap, although an alternative argument could be made that corrosion products and insoluble precipitation products such as iron metaborate or nickel iron borate could plug the gap and reduce the leakage to very low levels. At this stage, low levels of leakage from the annulus could manifest itself as the classic "popcorn" crust of boric acid deposits. Examples of boric

acid deposits from leaking CRDM nozzles are shown in Fig. 4. In contrast to other plants with leaking nozzles, the boric acid deposits on top of the D-B RPV head from leakage from CRDM flange joints could have acted as an "incubator" wherein leaking borated water is retained under the deposits. The identity of the boric acid species within the annular enclave is speculative and could have ranged from aqueous, concentrated solutions of boric acid to molten mixtures of boric acid and boric oxide. The oxygen content of the solution was presumably low, due to the limited access through the annular gap, coupled with the probable egress of superheated steam through the same gap and an uphill pressure gradient.

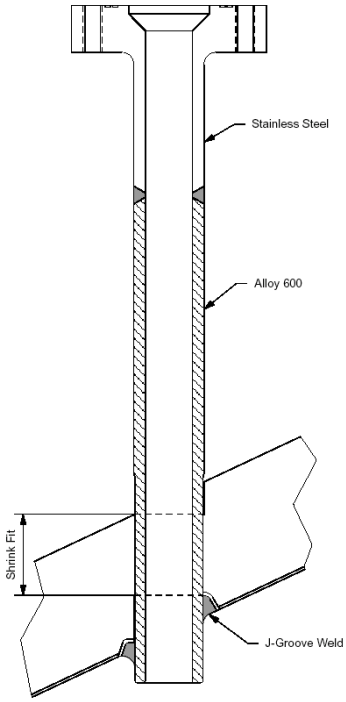

Figure 3.
Schematic of the Davis–Besse CRDM nozzle showing the SS flange, Alloy 600 penetration, and J–groove weld between the RPV head and the penetration.

Figure 4. Deposits of boric acid crystals on reactor pressure vessel head from leaking CRDM nozzles.

(c) *Late latency period.* As the crack continued to grow, the root cause report assumes that the annular gap increased in width and that because the growth in annulus width occurred over a substantial portion of the length around the annulus, the annulus flow area increased faster than the crack flow area. The report ignores any potential plugging of the annulus by corrosion products and insoluble precipitates, thus ensuring that the primary flow resistance would have been due to the dimensions of the crack and not to any restriction offered by the annulus geometry. Under these conditions, oxygen may enter the annulus.

(d) *Deep annulus corrosive attack.* In the scenario envisaged in the root cause report, continued widening of the annular gap would cause the velocity of flow out of the annulus, as well as the differential pressure, to decrease, allowing greater penetration of oxygen and increased corrosion rates. However, calculations of back-diffusion of oxygen against a flow stream presented at the EPRI meeting at Airlie House suggested that even very low flow rates would prevent such diffusion. The root cause report suggests that corrosion was likely to be greater near the crack (D-B nozzle #2) because leakage through the crack would maintain a fresh supply of new reactive oxidizing ions in the boundary layer near the corroding metallic surface.

(e) *Boric acid corrosion.* With high leakage rates, the annulus became filled with an increasing amount of moist steam, partially flashing as it exits. Heat transfer from the surrounding metal is no longer sufficient to immediately vaporize the portion of leakage that does not flash. The metal surface temperature was being suppressed by the cooling effect of the large heat flux required to vaporize the leaking coolant. This effect allowed a greater area to be wetted beneath the accumulations of boric acid. As the crack grew and the leak rate from the crack increased, the corroding annulus began to fill with a saturated boric acid solution. Because the wetted area would be the result of liquid flow, it would be expected to be predominantly downhill from the nozzle. This would result in high corrosion rates and wastage of RPV head material on the downhill side of the nozzle.

The root cause analysis report does not consider the conditions under which the initiation of circumferential cracks from the OD of the CRDM nozzle had occurred. The time line in the report assumes that the crack growth rates (CGRs) in the Alloy 600 are characteristic of those in pressurized water reactor (PWR) primary water. But a PWR primary water environment is not consistent with the observed degradation of the low-alloy steel.

Although it is not possible at present to establish the exact progression of mechanisms that led to the observed RPV head wastage, the degradation modes on the two extremes of the overall progression are known with reasonable confidence. At the extremely low leak rates ($\approx 10^{-6}$ to 10^{-5} gpm) observed in most of the leaking CRDM nozzles, the leaking flow completely vaporizes to steam immediately downstream from the principal flashing location. This results in a dry annulus and no loss of material.

The other extreme is associated with the classic boric acid corrosion mechanism caused by liquid boric acid solution concentrated through boiling and enhanced by oxygen available directly from the ambient atmosphere.[5] The extent of the boiling heat transfer associated with the relatively high leak rate of nozzle #3 was likely sufficient to cool the head enough to allow liquid solution to cover the walls of the cavity. It is clear that relatively high leakage rates from CRDM cracks are necessary for such catastrophic corrosion.

The D-B root cause report provides a scenario that attempts to explain the progression, but the differences between the D-B case and the other CRDM cracking instances are still unclear. The root cause report is incomplete in many regards, partially because much of the data necessary to support the hypotheses simply do not exist. Wastage of low-alloy steel in concentrated boric acid solutions is not well described or quantified in the literature, and especially not under the temperature, flow, and concentration of species that may have existed on the D-B head. The electrochemical potentials (ECPs) of the alloys in the aqueous solutions involved are not known.

This report presents experimental data on ECP and corrosion/wastage rates of the materials found in the RPV head and nozzles of the D–B reactor in boric acid solutions of varying concentrations at temperatures of 95–316°C (203–600°F). Tests were conducted in the following environmental conditions that have been postulated in the CRDM nozzle/head annulus: (i) high–temperature, high–pressure aqueous environment with a range of boric acid solution concentrations; (ii) high-temperature (150–300°C) boric acid powder at atmospheric pressure with and without addition of water; and (iii) low–temperature (≈95°C) saturated boric acid solution both deaerated and aerated. These correspond to the following situations: (a) low leakage through nozzle crack and nozzle/head annulus plugged, (b) low leakage through nozzle crack and nozzle/head annulus open, and (c) significant cooling due to high leakage through nozzle crack and nozzle/head annulus open. The results are compared with the existing corrosion/wastage data in the literature.

2. Experimental

2.1 Materials

Measurements of the ECP and corrosion rates have been performed on A533 Gr.–B low–alloy steel, Alloy 600, and austenitic Type 304 SS and Type 308 SS weld overlay, in boric acid solutions at temperatures between 95 and 316°C (203 and 600°F). The compositions of the alloys are given in Table 1.

Table 1. Composition of RPV head and nozzle alloys for corrosion studies

Alloy Type	Heat Number	Analysis	Composition (wt.%)									
			Ni	Fe	Si	P	S	Mn	C	N	Cr	Mo
A533 Gr.B[a]	Midland	Vendor	0.50	Bal.	0.17	0.014	0.016	1.28	0.200	–	0.19	0.47
	Lower Head	ANL	0.55	Bal.	0.28	0.025	0.010	1.27	0.220	–	0.19	0.50
304 SS[b]	53319	Vendor	8.88	Bal.	0.59	0.024	0.013	1.69	0.060	0.029	18.33	0.14
		ANL	8.96	Bal.	0.55	0.021	0.008	1.72	0.070	–	18.52	0.16
308 SS	–	Spec.	9-11	Bal.	0.90	0.040	0.030	2.5 max	0.080	–	18-21	0.75
		ANL	9.37	Bal.	0.56	0.027	0.002	1.27	0.029	–	21.08	0.39
Alloy 600[c]	NX8844B33	Vendor	Bal.	8.26	0.24	0.009	0.001	0.26	0.069	0.010	14.97	0.15
		ANL	Bal.	9.01	0.26	–	0.001	0.24	0.080	–	14.68	–

[a]162–mm thick hot–pressed plate from Midland reactor lower head. Austenitized at 871–899°C for 5.5 h and brine quenched; then tempered at 649–663°C for 5.5 h and brine quenched.
[b]Solution annealed pipe.
[c]25.4–mm–thick plate fabricated by INCO Alloys International, Inc., Huntington, WV, for the Electric Power Research Institute (EPRI). Annealed at 872°C for 1 h.

The size and shape of the specimens varied with the environmental conditions and type of test. Cylindrical rods with 3.2 or 6.35 mm (0.125 or 0.25 in.) diameter and up to 100 mm length were employed for ECP measurements and potentiodynamic studies. Ring specimens with 12.7 mm (0.5 in.) diameter and ≈3.2 mm (0.125 in.) wall thickness were used for the corrosion/wastage studies. A schematic drawing of shielded metal arc (SMA) weld overlay on A533 Gr.–B low–alloy steel plate using Type 308 SS filler metal is shown in Fig. 5. Cylindrical rod or ring specimens were fabricated from the weld overlay as shown in the drawing. A photograph of ring specimens and the weld overlay piece that was used for machining the specimens is shown in Fig. 6. Figure 7 shows specimen holder with a set of ring specimens of A533 Gr.–B steel and SMA weld overlay for corrosion/wastage studies in concentrated boric acid solutions at 100°C.

Figure 5. Schematic drawing of the Type 308 SS weld overlay on A533 Gr.-B low-alloy steel.

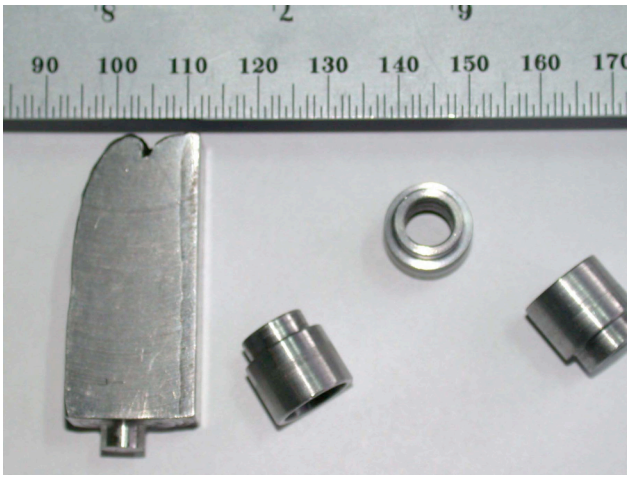

Figure 6.
Ring samples fabricated from the Type 308 SMA weld overlay.

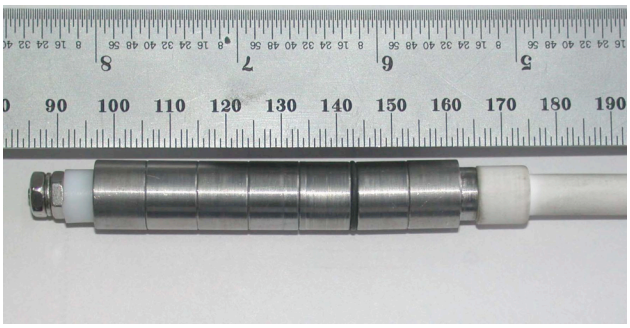

Figure 7.
Assembled set of ring samples of A533 Gr.-B low-alloy steel and Type 308 SS SMA weld overlay for corrosion/wastage tests.

2.2 Test Environments

The various test environments simulate the postulated conditions in the RPV head/nozzle crevice. The environment in the crevice between the RPV head and the Alloy 600 penetration above the J–groove weld (see Fig. 3) depends on what the leak rate is, and whether the nozzle/head annulus is plugged or open. The following three environmental conditions have been investigated in the present study: (i) low–temperature (≈95°C) saturated boric acid solution deaerated and aerated; (ii) high–temperature, high–pressure aqueous environment with a range of boric acid solution concentrations; and (iii) high-temperature (150–300°C) boric acid powder at atmospheric pressure with and without addition of water.

2.2.1 Low–Temperature Saturated Boric Acid Solutions

Near the end of the overall progression of damage, high leak rates through the CRDM cracks provide sufficient cooling of the metal surfaces to allow liquid boric acid solutions to form in the crevice. These solutions will become concentrated in boric acid through boiling and more reactive by infusion of oxygen available directly from the ambient atmosphere.

The solubility of boric acid[6,7] at temperatures up to 100°C (212°F) is shown in Fig. 8. The solubility increases by a factor of ≈8 when temperature is increased from room temperature (RT) to 100°C.

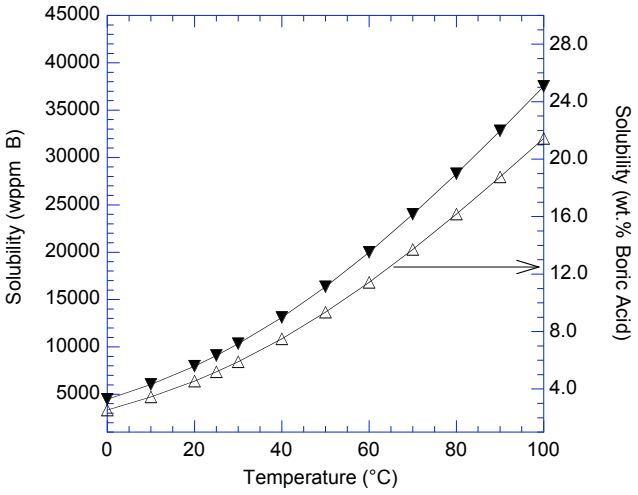

Figure 8.
Solubility of boric acid (wppm B or wt.% boric acid) in water vs. temperature (Ref. 6,7).

Figures 9a–d show the measured pH of aerated and deaerated solutions of boric acid at temperatures up to 100°C. The RT–saturated boric acid solution was prepared by adding more than the required amount of boric acid to ultra–high pure (UHP) water at RT and storing it for a few days. The temperature was measured using a three–digit Omega–digital K–type thermometer which was calibrated. The boiling point for the saturated boric acid solution was measured to be ≈103°C, but the experiments were conducted at 97.5°C. The 100°C–saturated solution was prepared by adding boric acid to UHP water at 100°C until excess boric acid crystals (or agglomerated powder) were presented in the solution. Boric acid solutions saturated at any other temperature between 25 and 100°C were obtained by cooling the 100°C–saturated solution. The solutions were purged with N_2 plus 1% H_2 gas for deaerated condition and were open to air environment for the aerated condition. The exact concentration of DO, measured by CHEMets ampoules, in the deaerated and aerated solutions was <5 and ≈30 ppb, respectively. The DO measurement was made by inserting a glass tip into the solution, opening the tip quickly at temperature to suck the solution, and closing the tip with a rubber cap. The test glass was air cooled to room temperature and DO measured by CHEMets capsules.

The pH of RT–saturated solution of boric acid is plotted as a function of temperature in Fig. 9a. The measured pH of both aerated and deaerated solutions show little or no change with temperature at 25–100°C. The pH of boric acid solutions that were saturated at temperature is plotted as a function of temperature in Fig. 9b and boron concentration in Fig. 9c; the pH decreased with increasing temperature or boron concentration. The pH and solubility of boric acid (wppm B) in water are plotted as a function of inverse temperature in Fig. 9d to gain an understanding of the solution enthalpy for the boric acid in the water and formation energy for the ionization, i.e., $2H_2O + B(OH)_3 = [H_3O]^+ + [B(OH)_4]^-$. The results indicate that the $[B(OH)_4]^-$ ion is stable in the temperature range 25–100°C, and boric acid may be treated to be totally ionized in solutions that are saturated at test temperature.

Another scenario can also create low–temperature saturated solutions of boric acid. Slow leakage into an open crevice or annulus leaves deposits of boric acid in the crevice and also on top of RPV head surfaces (Fig. 4). The annulus between the nozzle and head is then plugged by deposits and/or corrosion products. In the absence of moisture, these deposits will be relatively dry and a layer of molten HBO_2 and solid B_2O_3 will form next to the hot metal surface. Later moisture may be introduced to this pile of deposits either due to unplugging of

the nozzle/head annulus or leakage from the CRDM nozzle flange or continued leakage through the crack. The heat of evaporation will provide cooling and, if the rate at which moisture is added to the pile of deposits is equal to the rate at which moisture evaporates, a concentrated solution of boric acid will form under the pile; the solution temperature may be as high as 150 or 170°C.

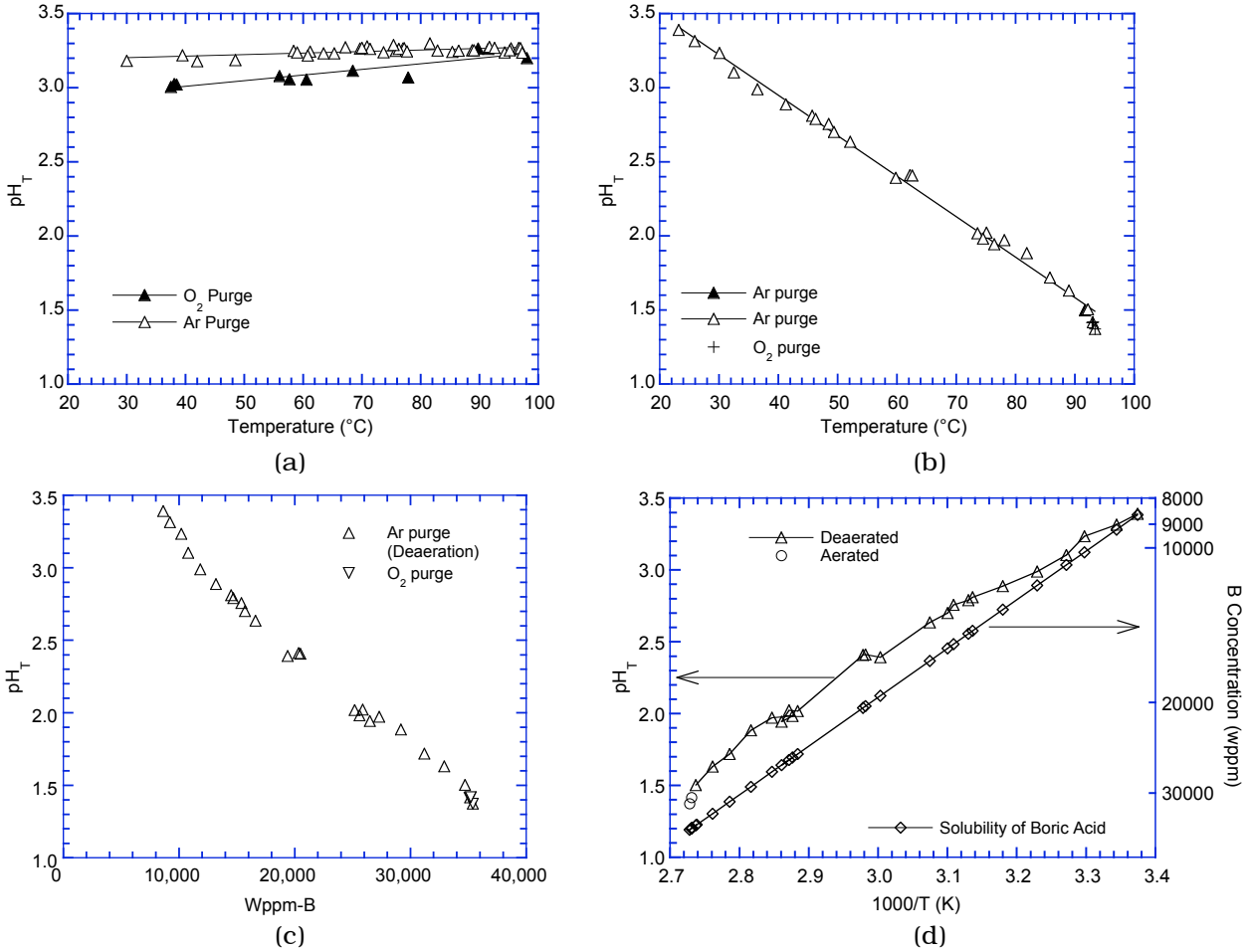

Figure 9. Plots of pH_T vs. temperature in the oxygen and argon gas environments (a) for the RT–saturated solution and (b) the boric acid saturated at T; (c) pH_T vs. wppm B for temperature between RT and 100°C; and (d) pH_T and wppm B vs. inverse temperature.

2.2.2 High–Temperature High–Pressure PWR Environments

Initially, extremely low leak rates result in complete flashing of the coolant to steam. Under this condition, two scenarios are possible based on whether the nozzle/head annulus is plugged by deposits and/or corrosion products or is open to the atmosphere. A plugged nozzle/head annulus will result in a high–temperature, high–pressure aqueous environment in the annulus, i.e., on the OD of the CRDM nozzle. The PWR environment used in the present study consisted of 1000 ppm B, 2 ppm Li, <10 ppb dissolved oxygen (DO), and ≈2 ppm (≈23 cc/kg) dissolved hydrogen. However, depending on how long after the leak that the crevice gets plugged, the concentrations of B and Li in the solution may be significantly greater than the typical values in the PWR environment. Continued leakage into an open crevice will cause a buildup of boric acid deposits in the crevice.

2.2.3 Molten H–B–O Environments at Ambient Temperature

A crevice open to the atmosphere would cause deposits of boric acid on hot metal surfaces (typically at temperatures above 300°C). However, at high temperatures boric acid loses moisture and transforms first to HBO_2 at 169°C and then to B_2O_3 at temperatures above 300°C. The various phases for the H-B-O system at temperatures up to 450°C are listed in Table 2. HBO_2 is molten at temperatures above 236°C and, in the absence of moisture, readily transforms to solid B_2O_3 at temperatures in excess of 300°C; B_2O_3 melts at 450°C. Consequently, deposits of boric acid in contact with hot RPV head surfaces would consist of a mixture of molten HBO_2 and solid B_2O_3.

Table. 2. Melting points and phase transition temperatures in the H-B-O system.

Phases	Temperature (°C)	Reaction with H_2O
H_3BO_3 or $B(OH)_3$	169 (Transition)	$B(OH)_3 + H_2O = [B(OH)_4]^- + H^+$
HBO_2	236 (Melting)	$B(OH)_3 - H_2O = HBO_2$
B_2O_3	300 (Transition), 450 (Melting)	$2HBO_2 - H_2O = B_2O_3$

The moisture content of the H-B-O system is expected to be an important parameter for corrosion studies, since the stability and the presence/absence of a given phase are dictated by the addition or removal of water, as can be seen by the reactions given in Table 2. The temperature dependence of the equilibrium water vapor pressure (pH_2O), calculated for various reactions in the H-B-O system, is shown in Fig. 10. The equilibrium water vapor pressure was calculated using the two equations shown in the figure and thermodynamic data from Ref. 8. Conversion of boric acid into HBO_2 and HBO_2 into B_2O_3 requires removal of H_2O, and maintenance of mixtures of boric acid and HBO_2 or HBO_2 and B_2O_3 dictated significant increases in steam pressure, especially at higher temperatures. Later in this report we discuss various experiments that were conducted to examine the corrosion performance of A533 steel in different H-B-O compounds.

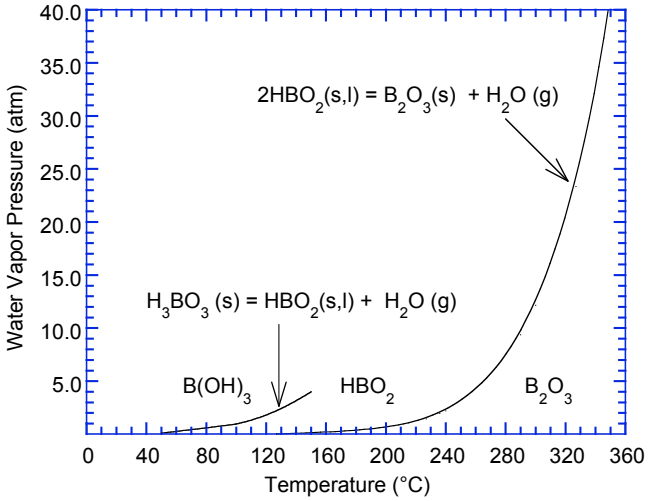

Figure 10.
Plot of equilibrium water vapor pressure vs. temperature for the H-B-O system.

2.3 Test Facilities

2.3.1 Low–Temperature Tests at Ambient Pressure

The electrochemical cell used for the ECP and potentiodynamic measurements in concentrated solutions of boric acid at 95°C (203°F) and ambient pressure is shown in Fig. 11. The cell consists of a 1–L round–bottom Pyrex flask that was modified by the addition of various necks to permit introduction of working, counter, and reference electrodes, pH probe, gas inlet and outlet tubes, and a thermocouple. A saturated calomel electrode (SCE) utilizing a porous plug tip was used as the reference electrode, and a platinum sheet as auxiliary or counter electrode. A Luggin capillary with salt–bridge connection to the reference electrode separated the bulk boric acid solution from the saturated calomel reference electrode. The probe tip could be easily adjusted to bring it in close proximity with the working electrode. A 6.35–mm diameter and 75–mm long rod was used as a working electrode (Fig. 12). The working electrode was tightly intruded with vacuum grease into a PHARMA–50 (Dow Corning) tubing such that only the bottom surface (0.317 cm^2 area) of the electrode was exposed to the solution. The bottom surface was polished with a 600–grit silicon carbide paper.

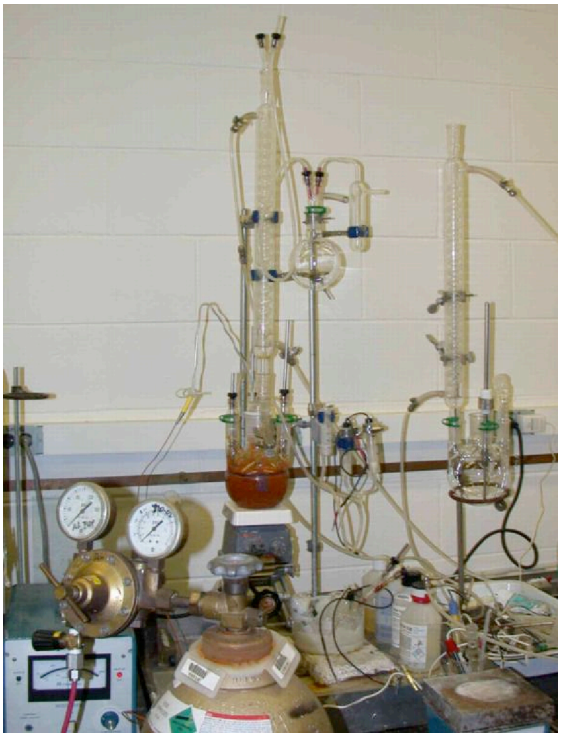

Figure 11. Electrochemical cell for potentiodynamic studies.

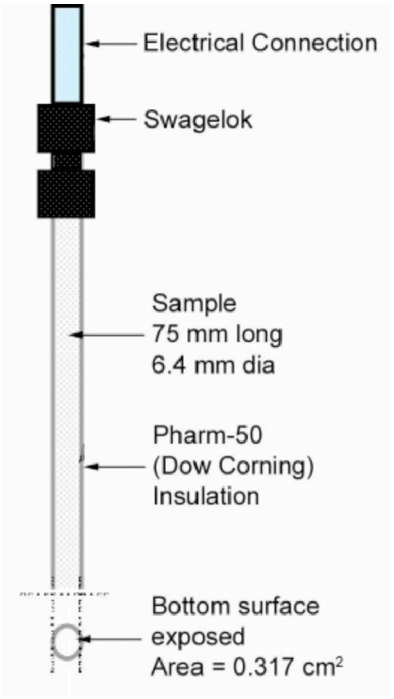

Figure 12. Schematic drawing of the working electrode.

A scanning potentiostat with high input–impedance (10^{12} Ω) was used for the potentiodynamic measurements. The potential was automatically varied at a constant rate between two preset values, and the current and potential were recorded continuously. The tests were conducted in accordance with ASTM Standard Procedure G5–94.[9] A potential scan rate of 0.16 mV/s was used for the test runs; a fast scan rate of 5 mV/s was used to measure the open circuit potential and establish the test conditions. The apparatus was calibrated using a Fe working electrode. The results are presented in Fig. 13. The measured corrosion

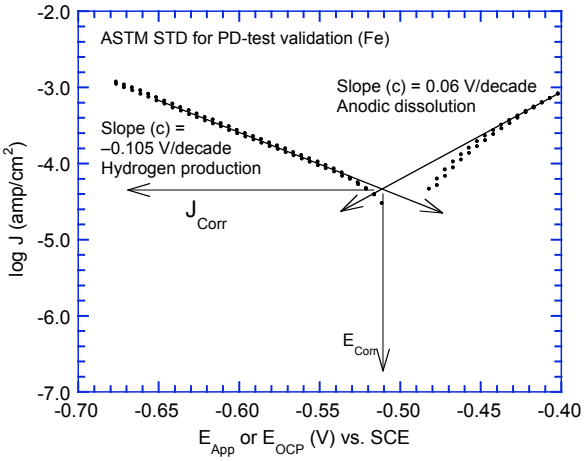

Figure 13.
Calibration of the potentiodynamic test apparatus following with ASTM G5-94 using Fe working electrode and saturated calomel reference electrode.

potential for Fe, –0.512 V, is in good agreement with the standard value of –0.52 V quoted in ASTM G5–94 in terms of SCE. The measured potentials, E_{meas} (V), may be converted to the standard hydrogen electrode (SHE) scale, E_{SHE} (V), by the expression[10]

$$E_{SHE} = E_{meas} + 0.242 - 7.6x10^{-4}\,\Delta T \qquad (1)$$

where ΔT(°C) is the temperature difference of the salt bridge in the reference electrode (i.e., the test temperature minus ambient temperature).

The apparatus used for corrosion/wastage studies on ring specimens of A533 Gr.–B low–alloy steel, Alloy 600, and Type 308 SS cladding, in concentrated solutions of boric acid at temperatures up to 100°C is shown in Fig. 14. The specimens were rotated at 50 rpm, and material loss or wastage was measured at 24, 76, 100, 311, and 411 h. To prevent possible

Figure 14.
Apparatus for corrosion test in concentrated solutions of boric acid at temperatures up to 100°C.

galvanic interaction, the specimens were separated from each other with an insulator (Teflon gasket) and isolated from the specimen holder by tygon tubing.

The solution was prepared by dissolving 158–g boric acid in 500–mL water at 95–100°C; this is ≈3 g in excess of the estimated solubility of boric acid at 95°C. For ECP and potentiodynamic measurements, the DO in solution was fixed by bubbling air through the solution prior to the test, and for corrosion tests, the solution was open to air. The measured DO content was 600 and 30 ppb, respectively, after bubbling air and when the system was open to air. It seems the DO in the saturated boric acid solution is substantially lower than normally would be present in high–purity water (≈2 ppm). The test specimen was degreased and rinsed in distilled water before immersion into the cell; the salt–bridge probe tip was adjusted to ≈2 mm from the test specimen. Open circuit or corrosion potential was recorded ≈1 h after immersion. Tests were performed on A533 Gr.–B low–alloy steel, Alloy 600, and Type 304 and 308 SS in aerated saturated solution of boric acid at 95°C.

2.3.2 High–Temperature High–Pressure Tests

Figure 15 shows a schematic diagram of the facility for potentiodynamic and ECP measurements in high–pressure solutions of boric acid of varying concentrations at temperatures up to 300°C. The facility consists of a supply tank, high–pressure pump, preheater, heated test chamber, regenerative heat exchanger, Mity Mite™ back-pressure regulator, and drain. The entire system from the storage tank to the drain, including the 25 x 50 mm cross section and 75 mm long test chamber, was constructed of Type 304 SS. Figure 16 shows the configuration of the test chamber with solution inlet/outlet lines, working electrode assembly, Pt counter electrode, 0.1–M KCl/AgCl/Ag external reference electrode, and a thermocouple well. The working electrode assembly consisted of three 3.2–mm (0.125–in.) diameter x 3.2–mm (0.125–in.) long samples of A533 Gr.–B, Alloy 600, and Type 308 weld metal, spot welded to Pt lead wires, plus a fourth Pt wire sample. The lead wires were covered

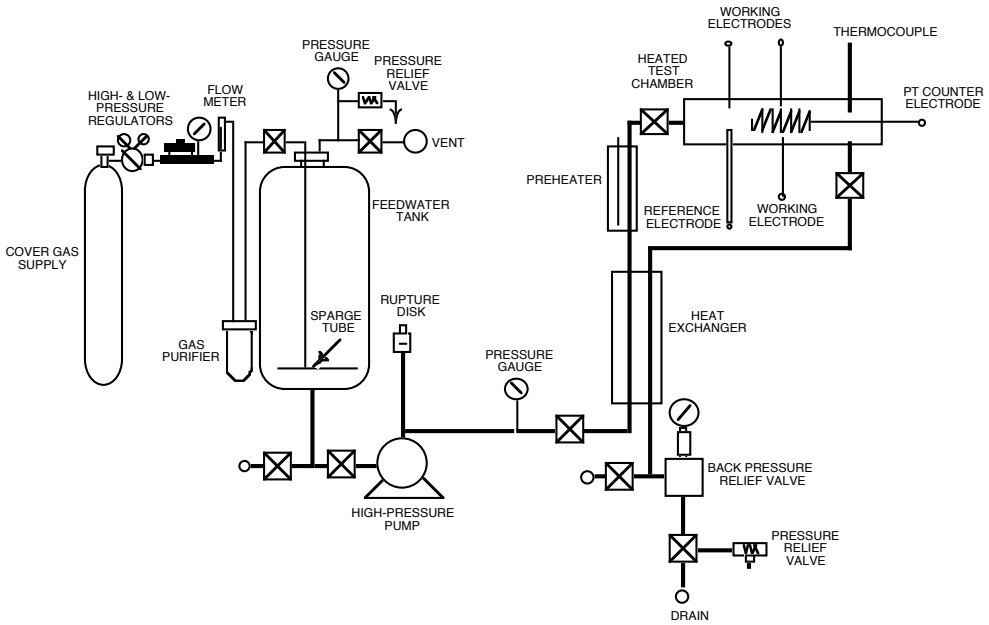

Figure 15. Schematic of the facility for high–temperature high–pressure tests in PWR environments with various concentrations of B and Li.

with teflon spaghetti and secured in a four-hole alumina rod, 9.5–mm (0.375 in.) diameter 127–mm (5 in.) long, such that only the working electrode samples were exposed to the test solutions, Fig. 17.

The simulated PWR solution, consisting of high–purity water containing <10 ppb DO, 1000–9000 ppm B, and ≈2 ppm Li, was circulated through the system at a relatively low flow rate of ≈10 mL/min. The high–purity water was prepared by passing deionized water through a set of filters that comprise a carbon filter, an Organex–Q filter, two ion exchangers, and a 0.2–mm capsule filter. The DO level in the water was reduced to <10 ppb by bubbling pure N_2 and then pure H_2 through the water. The DO level was measured in the feedwater tank and the effluent with a Model 26075 (sensor 21152) Orbisphere DO sensor and monitor. The desired amount of boric acid and lithium hydroxide were dissolved in 20 L of deionized water and this solution was then added to the supply tank to prepare the test solutions.

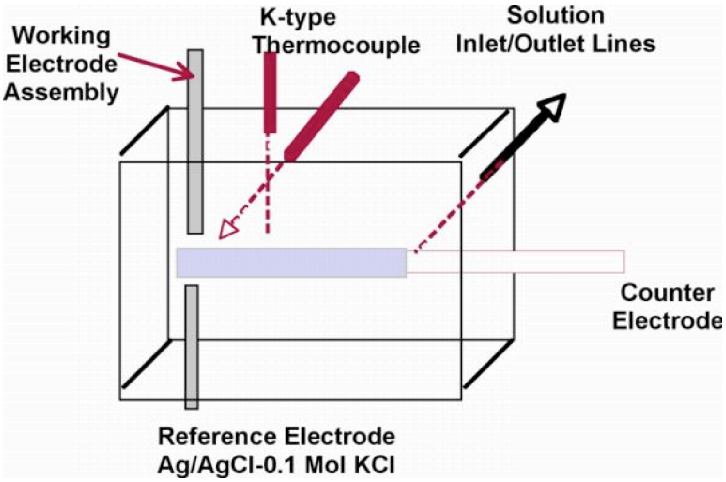

Figure 16. Schematic of the test chamber showing the location of various electrodes, solution inlet/outlet lines, and thermocouple well.

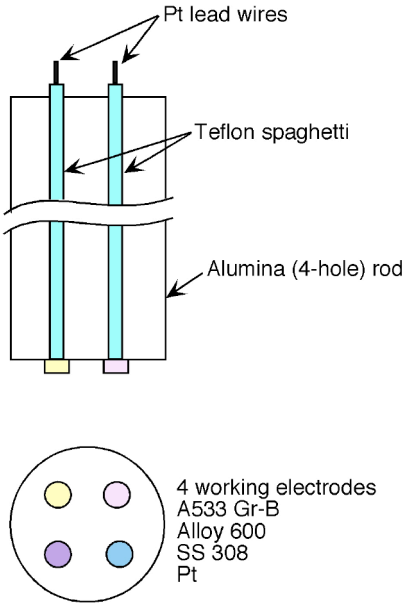

Figure 17. A four hole high–purity alumina rod containing four working electrodes.

The corrosion/wastage rates of A533B low–alloy steel, Alloy 600, and Type 308 SS cladding were performed in boric acid solutions of varying concentrations at 95–316°C (203–600°F). The concentration of B in the solutions ranged from the typical value for normal PWR water, e.g., 1000 wppm, to RT–saturated boric acid solution containing 9090 wppm B. All solutions contained 2 wppm Li, and a 34–kPa overpressure of pure H_2 was maintained above the supply tank to obtain ≈2 ppm (≈23 kg/cc) dissolved H_2 in the solution. A schematic diagram of the specimen holder and disc–shaped specimens used for the study is shown in Fig. 18. Specimens, 6.4–mm (0.25–in.) diameter and 1-mm thick, were supported by an alumina rod and connected with 0.25–mm (0.01–in.) diameter SS wire. After the tests, specimen weight was measured to determine corrosion rates. The specimens were also examined by scanning electron microscopy and energy-dispersive x-ray spectroscopy (SEM/EDS); x-ray diffraction studies were also conducted for some A533 Gr.–B specimens.

Figure 18. Schematic of the test specimen holder for high-temperature, high-pressure corrosion tests in a flowing boric acid solution under the hydrogen cover gas.

2.3.3 Tests in Molten H–B–O Environment at Ambient Pressure

The facility used for potentiodynamic and ECP measurements in molten HBO_2/B_2O_3 environments at 240 and 290°C and ambient pressure is shown in Fig. 19. The melt was prepared in a 125–mL Type 304 SS beaker with its lip cut off. The test beaker was placed inside a 1.2–L SS environmental chamber, alumina blocks were used to provide electrical insulation between the two vessels. The environment above the test vessel was controlled by a constant supply of Ar or air through the environmental chamber.

For each potentiodynamic or ECP measurement, ≈300 g of boric acid was used to prepare ≈40–mm–deep (≈1.6–in.) melt in the test vessel. Typically, only 100 g boric acid could be melted in the 125 mL beaker. The process was repeated three times to collect the total volume of melt for each test. The molten salt was totally transparent and appeared like clear glass.

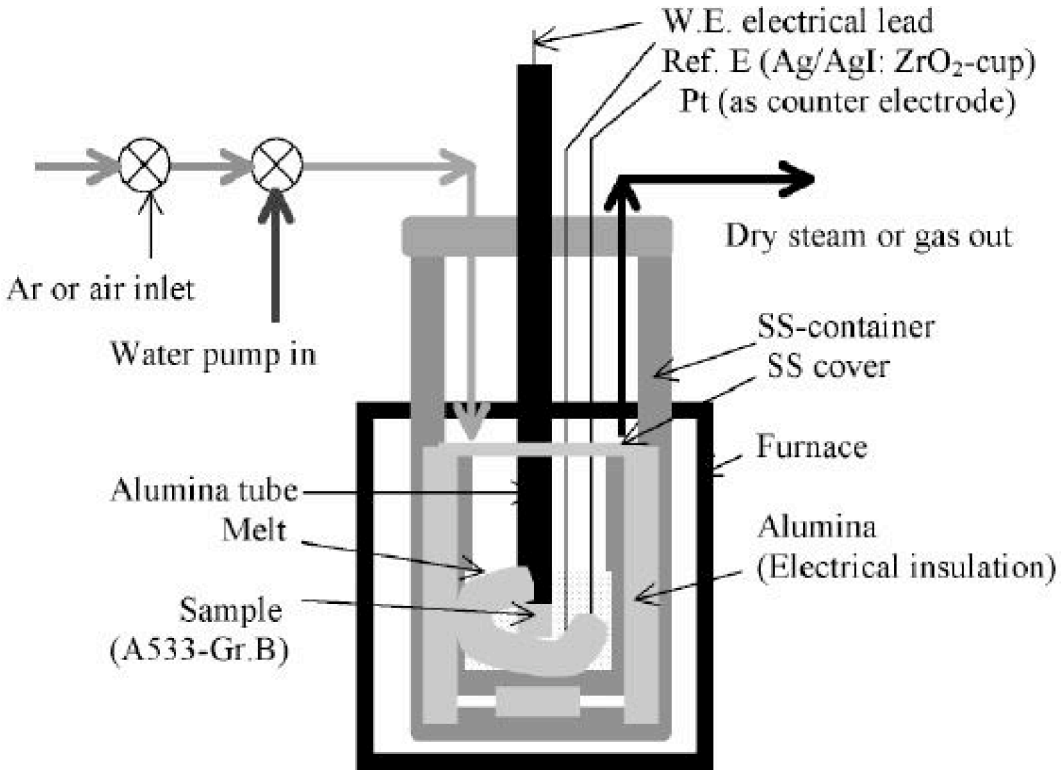

Figure 19. Schematic of the facility for potentiodynamic and ECP measurements in mixtures of molten boric acid and boric oxide at temperatures up to 300°C.

As discussed earlier, when heated, boric acid transforms first to HBO_2 and then to B_2O_3; it loses weight as H_2O evaporates. This is demonstrated in Fig. 20, which shows the thermogravimetric analysis (TGA) for a 180–mg sample of boric acid as it was heated from 25 to 420°C in air. After ≈1500 s the sample exhibited an erratic behavior in weight change due to formation and escape of bubbles from the melt. The results indicate that at up to 350°C the observed sample weight is in agreement with the expected weight for the B_2O_3 phase. At temperatures >350°C the sample weight decreased further; additional tests are needed to examine the phase stability at higher temperatures. The change in weight with time of another ≈100–g sample of boric acid at 280°C in air is shown in Fig. 21; the estimated weights for HBO_2 and B_2O_3 are identified in the figure.

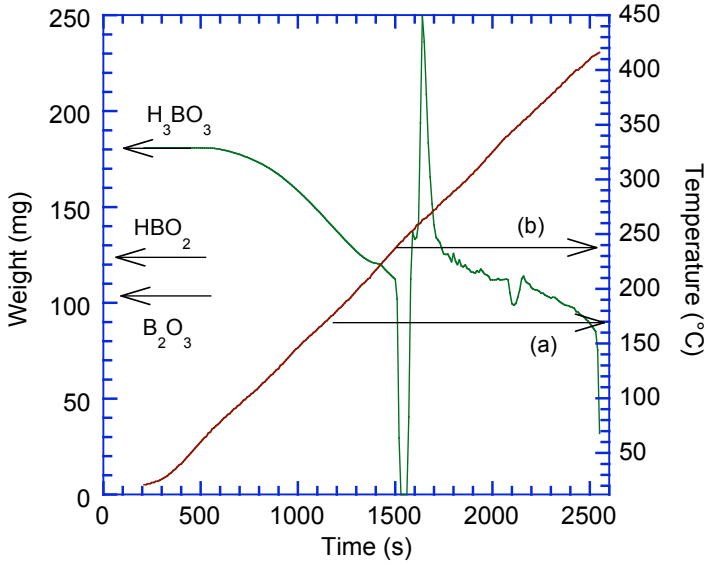

Figure 20.
Change in weight of boric acid when heated from 25 to 450°C in an air environment, (a) corresponds to transition to HBO_2 and (b) represents melting point of HBO_2.

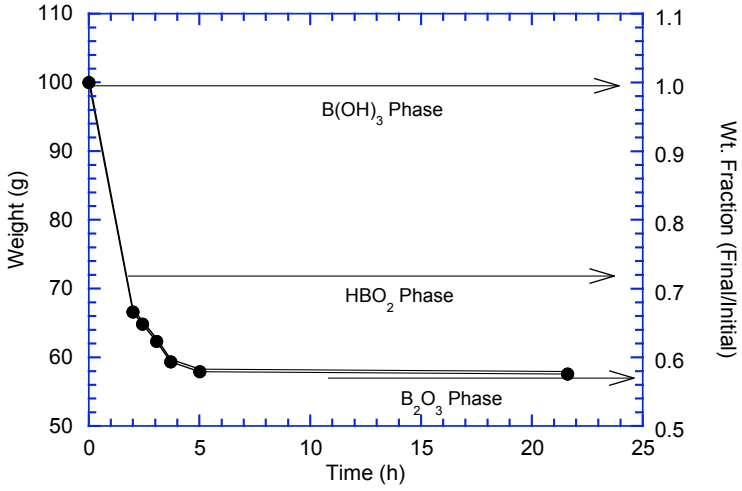

Figure 21.
Weight change vs. time at 280°C in air atmosphere. Boric acid turns to HBO_2 and mostly B_2O_3 phase.

Figure 22 shows the schematic diagram of the working electrode used in the present study. It consists of a 6.4–mm (0.25–in.) diameter x 6.4–mm (0.25 in.) long sample of A533 Gr.–B steel spot welded with silver to a SS lead wire and inserted into the end of a 6.4–mm (0.25 in.) OD alumina tube. A heat sink was used during welding to prevent overheating of the sample. The welded end of the electrode was carefully machined to provide a

leak–tight seal with the alumina tube. The total area of the working electrode exposed to the solution was 2.3 mm^2. A 3–mm wide Pt strip was used as counter electrode. The reference electrode (shown in Fig. 23) consisted of Ag/AgI electrolyte contained in a porous ZrO_2 cup. The AgI electrolyte was allowed to soak into the ZrO_2 cup at 700°C for ≈600 s before contact with the H-B-O melt. The activity of AgI in solid state is unity, and at >147°C AgI becomes an ionic conductor with a transport number for Ag of 1.

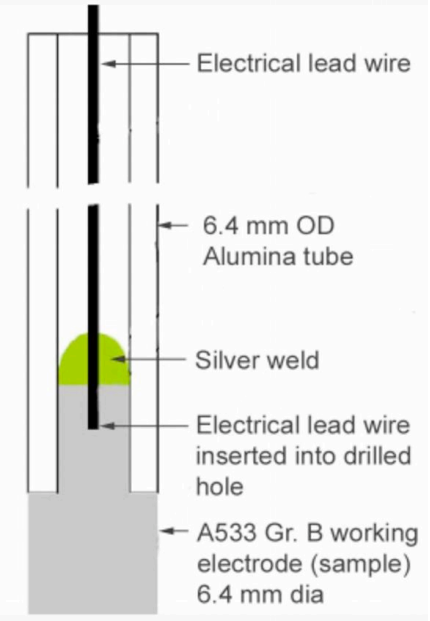

Figure 22. A533 Gr.–B low–alloy steel working electrode.

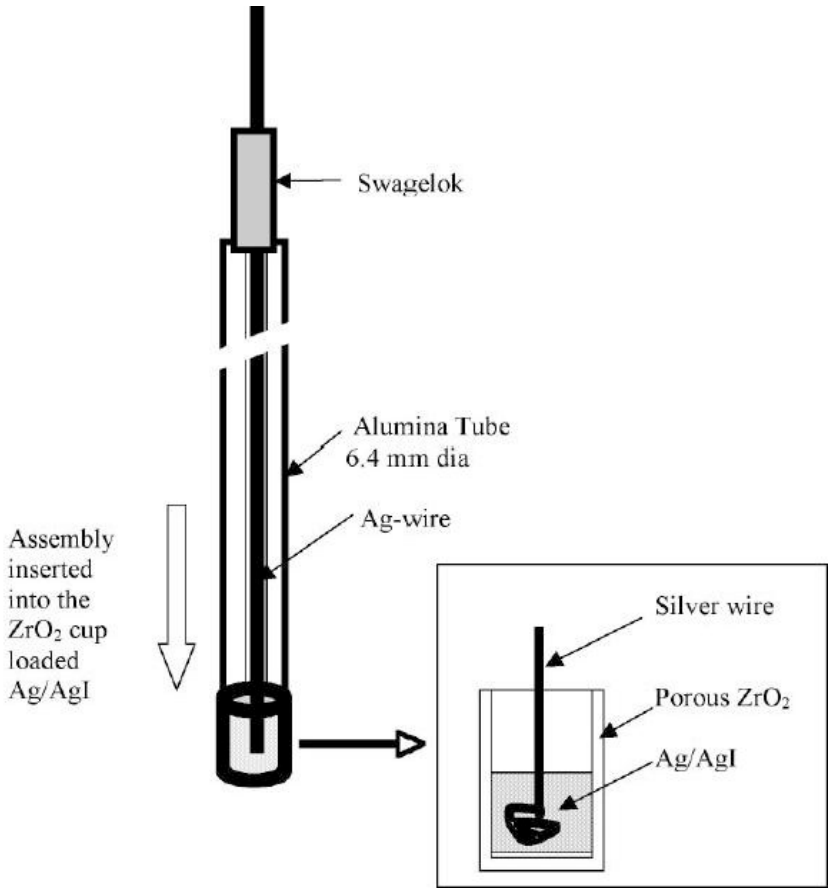

Figure 23. Reference electrode consisting of Ag/AgI electrolyte contained in a porous sintered ZrO_2 cup.

Figure 24 shows the apparatus for conducting corrosion tests in boric acid powder at 150–300°C, with and without the addition of water. It consists of a 63.5–mm (2.5–in.) diameter, 572–mm (22.5–in.) long SS chamber, the bottom ≈250 mm (10 in.) of which was heated in a furnace. A long 6.35-mm (0.25–in.) diameter SS tube was used both as the specimen holder and for addition of water to the system. A stack of three ring samples was mounted at the end of the tube; the stack was rotated at ≈50 rpm during the test.

For each corrosion test, the SS chamber was densely packed with boric acid powder to a depth of ≈356 mm (≈14 in.). A stack of samples was inserted into the boric acid powder by slowly rotating the stack and pushing it in. The furnace was then heated to 300°C to create a temperature gradient in the column of boric acid powder inside the test chamber; the temperature of the column was monitored at 6 locations. Under steady state the top of the

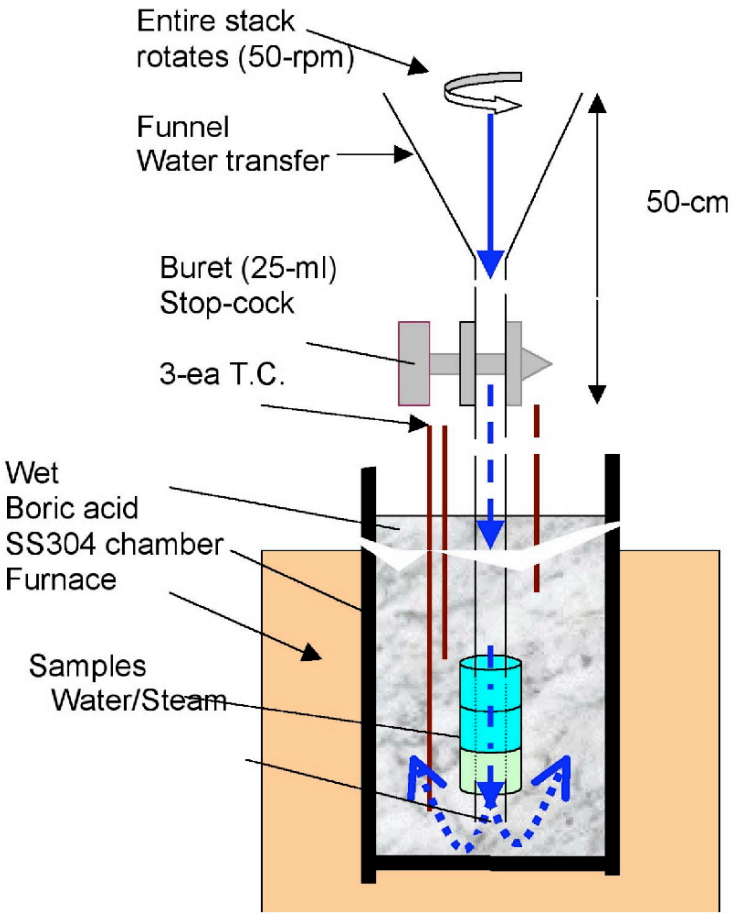

Figure 24.
The apparatus for conducting corrosion tests in molten H-B-O system with water additions.

column was at room temperature and the bottom at 300°C. Based on the information presented in Table 2 and Fig. 10, the environment at different depths of the test chamber is expected to be a molten mixture of B_2O_3 + HBO_2 at 300°C, molten HBO_2 at 260°C, and a dry powder of HBO_2 + H_3BO_3 at 150°C. For the tests without addition of water, a stack of ring specimens was exposed for 24 h in these three temperature zones.

A similar procedure was followed for the corrosion tests with addition of water. A densely packed column of boric acid with a stack of corrosion specimens was heated at the bottom to 300°C. Then, 200–250 mL of water was poured into the system through the specimen holder tube. After the initial reaction when water flashed to steam, the system cooled rapidly, and the entire column of boric acid in the test chamber was covered with water. Additional water was added on top of the boric acid to ensure that the entire column of boric acid powder/melt was covered with water for the duration of the test. Under steady state, the test chamber consisted of saturated solution of boric acid at room temperature at the top of the chamber and at 150 or 170°C at the bottom of the chamber. A photograph of the solid boric acid crust that was left at the bottom of the test chamber after the corrosion test with water addition is shown in Fig. 25.

Figure 25.
Photograph of the solid boric acid crust left at the bottom of the test chamber after the corrosion test with water addition.

2.3.4 Capsule Test

Capsule corrosion tests were conducted on A533 Gr.–B, Alloy 600, and Type 308 SS samples to study corrosion under equilibrium conditions in the H-B-O system at high temperatures and pressures. The test capsule consisted of a heavy-wall Type 304 SS tube, 12.7 mm (0.5 in.) diameter and 50 mm (2 in.) long, enclosed with Swagelok caps at each end, Fig. 26. The capsules heated to 294 and 316°C had bulged significantly because of buildup of high pressure inside the capsules that were heated to high temperatures. Disk–shaped samples, 6.35 mm (0.25 in.) diameter and 0.25 mm (0.01 in.) thick, were used for the tests. The capsules were filled with room–temperature saturated boric acid solution, and were sealed and heated to temperatures between 170 and 316°C in an Ar–purged furnace. All corrosion tests were of 68–h duration. The samples were removed from the capsules after the tests, ultrasonically cleaned in ethanol, and examined by SEM and X-ray analysis.

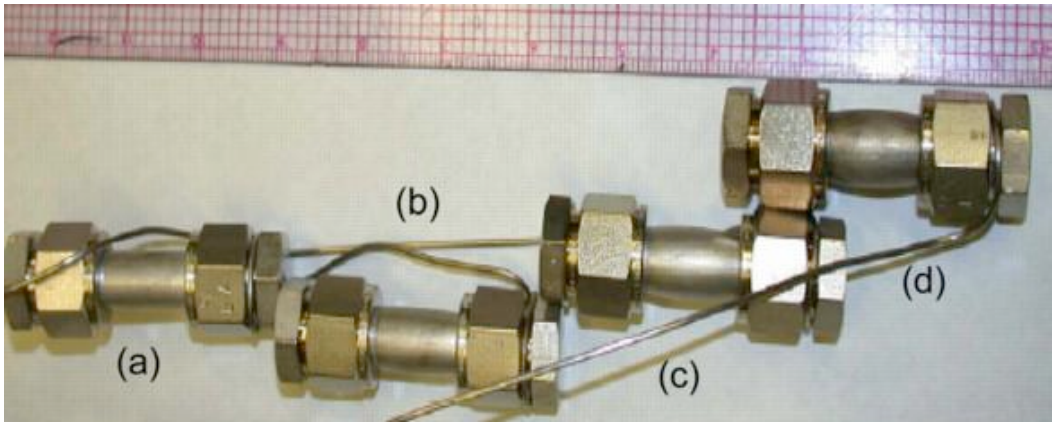

Figure 26. Test capsules 12.7 mm (0.5 in.) in diameter and 50 mm (2 in.) long, loaded with a boric acid solution saturated at room temperature and tested at (a) 172°C, (b) 235°C, (c) 294°C, and (d) 316°C.

3. Results

3.1 ECP and Potentiodynamic Measurements

3.1.1 Low–Temperature Tests at Ambient Pressure

The ECP of A533 Gr.–B, Alloy 600, and 308 SS clad were measured in saturated boric acid solution at ≈95°C and ambient pressure. Typical plots of ECP vs. time for the three materials are shown in Fig. 27. The results show a large increase in the ECP of 308 SS clad and a slight increase for Alloy 600 within the few hours of exposure; the ECP of A533 Gr.–B steel is lower than the other alloys and did not change with time. The increase in ECP of 308 SS clad and Alloy 600 is due to the formation of a protective oxide layer, whereas the surface of A533 Gr.–B steel stays bare, indicating dissolution or corrosion. The ECPs of A533 Gr.–B steel, Alloy 600, and 308 SS clad in boric acid solutions with different B content at 95°C and ambient pressure are compiled in Table 3.

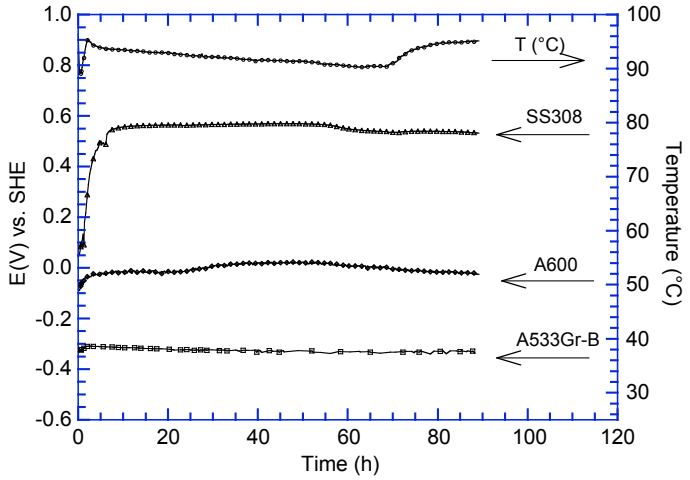

Figure 27.
Typical plot of measured ECP vs. time for the A533 Gr.-B, Alloy 600, and 308 SS in saturated boric acid solution at ≈95°C and ambient pressure.

Table 3. The ECP of A533 Gr.–B, Type 304 SS, 308 SS weld metal, and Alloy 600 in boric acid solutions at 95°C and ambient pressure.

B Content (wppm)	Gas Environment	ECP (V vs. SHE)			
		A533 Gr.–B	308 SS Weld	304 SS	Alloy 600
36,00	Aerated	-0.332	0.478	0.314	0.151
	Deaerated	-0.296	–		
9,09	Aerated	-0.295	–		
3,56	Aerated	-0.433	–		
	Deaerated	-0.450	–		

Several potentiodynamic tests were also performed on A533 Gr.–B low–alloy steel, Alloy 600, and Type 304 SS in aerated and deaerated solutions of boric acid containing 3500 or 36,000 wppm B at ≈95°C. Figure 28 shows the current density vs. applied potential (vs. SHE) plots for Type 304 SS in aerated saturated solution of boric acid containing 36,000 ppm B at 95°C. The results show a plateau, indicating passivation. For austenitic SSs and Alloy 600, because of changes in the surface condition, the corrosion potential typically shifts to a higher value after passivation.

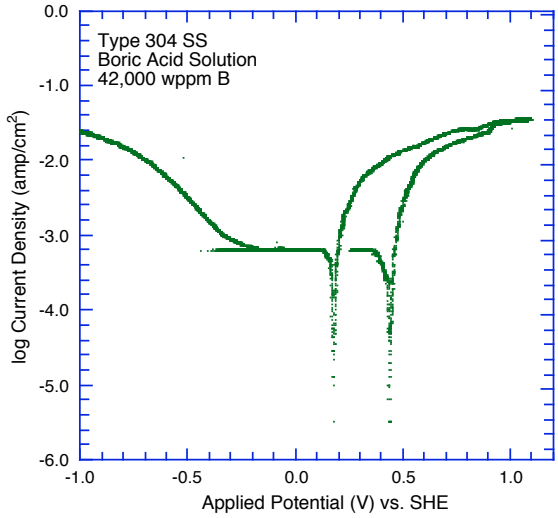

Figure 28.
Potentiodynamic test results for Type 304 stainless steel in aerated saturated solution of boric acid (36,000 wppm B) at ≈100°C.

Figure 29 shows the potentiodynamic test result for the A533 Gr.–B low–alloy steel in the aerated saturated boric acid solution at ≈95°C. The A533 Gr.–B low–alloy steel did not show any passivation behavior. Even after several potential scan cycles, corrosion potential remained the same. Corrosion rates were estimated from the current density vs. potential plots using Faraday's law and the $Fe \rightarrow Fe^{+2} + 2e^{-}$ reaction. The corrosion current density obtained from the potentiodynamic test, i.e., J_{corr} = 4 mA/cm^2 at E_{corr} = -0.342 V (SHE), agrees well with the corrosion rates obtained from corrosion/wastage tests discussed in the next section. The significant results from these tests are summarized below.

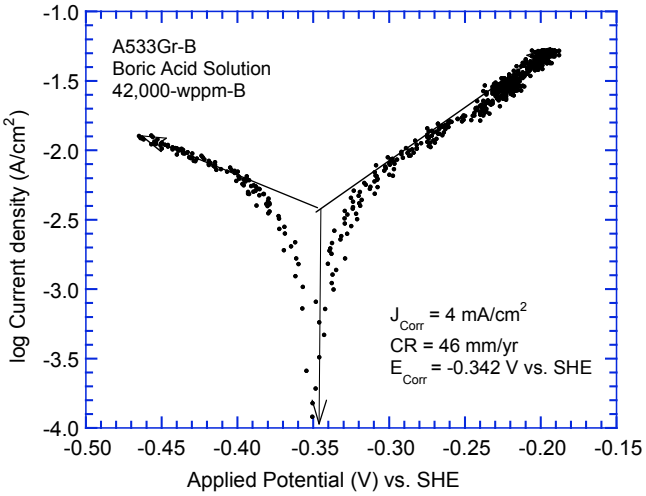

Figure 29.
Potentiodynamic test results for A533 Gr.–B steel in an aerated saturated boric acid solution at 95°C.

For tests in boric acid solution with 36,000 wppm B, the aerated solution turned reddish brown after the test and contained dark brown particles, whereas the deaerated solution remained colorless and contained dark magnetic particles. The solubility of boric acid in water at ≈95°C is slightly greater in deaerated than aerated solutions. Estimated corrosion rates were a factor of ≈3 higher in aerated solution than deaerated solution.

For tests in boric acid solution with 3500 wppm B, both aerated and deaerated solutions remained colorless and contained dark magnetic particles that were identified by x–ray

diffraction analyses as a mixture of maghemite (γ–Fe_2O_3) and magnetite (Fe_3O_4). The A533 Gr.–B low–alloy steel developed a very rough, black, and porous surface layer, whereas a thin, loosely–adherent white film was formed on Type 304 SS and Alloy 600. X-ray diffraction analyses indicated mixtures of boric acid, Fe_2O_3 iron oxide (maghemite–C or γ Fe_2O_3 and hematite), and iron borate FeB_2O_4, on the surface of A533–Gr. B steel. Nickel oxide (NiO), nickel chromium oxide ($NiCr_2O_4$), and nickel–oxide–hydroxide were identified on the Alloy 600 specimen. The A533–Gr. B steel exhibits a heavily reacted porous surface, shown in Fig. 30. Estimated corrosion rates were a factor of ≈1.5 higher in aerated solution than in deaerated solution.

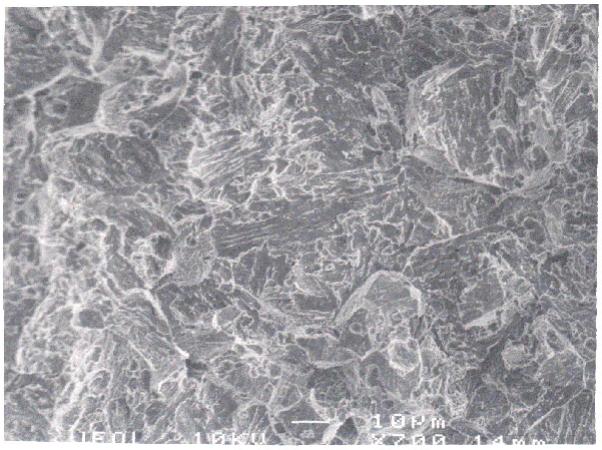

Figure 30.
Photomicrograph of A533 Gr.–B low–alloy steel tested in deaerated boric acid solution containing 3500 wppm B at 95°C.

3.1.2 Tests in Molten H–B–O System at Ambient Pressure

Figure 31 shows the result of a potentiodynamic test on A533 Gr.–B steel in the H–B–O system at 290°C. The H-B-O melt was equilibrated at 290°C for ≈12 h in air. The measured current density throughout the test indicates a very protective surface layer; the results indicate that in the absence of moisture, A533 Gr.–B steel would show negligible corrosion in molten HBO_2.

Figure 32 shows the scenario that occurs during a potentiodynamic test conducted in the H–B–O system with addition of water. It gives a representation of current density as a function

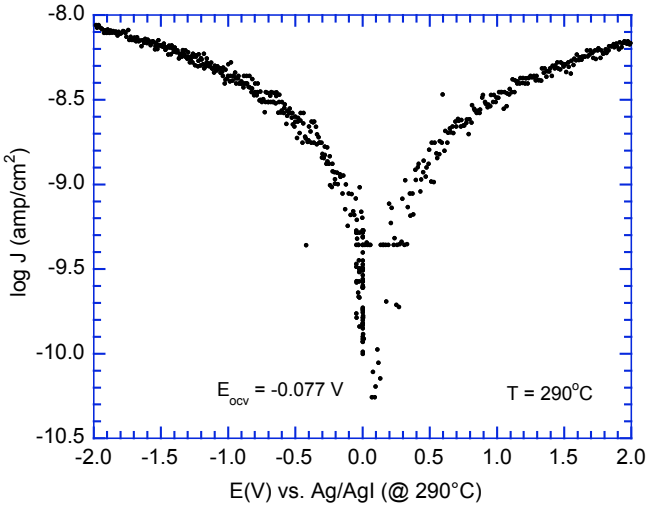

Figure 31.
Potentiodynamic test on A533 Gr.–B steel in molten H-B-O system at 290°C.

of sweeping voltage between +2 to –2. The experiment was started at 290°C with water injection, and the current density increased significantly when the water was introduced into the chamber (depicted by Regions "1" and "2" in Fig. 32). At +2 V, the sweeping direction was reversed till the voltage reached –2 V (Regions 3 and 4), at which point the volatgae direction was reversed again and continued sweeping (Regions 5 through 8). As the moisture evaporates, the current density decreased to a low value similar to that observed in a dry system. (Note that the temperature in the system during the experiment could not be maintained constant due to the addition and evaporation of moisture.) The experiment does show that a significant increase in current density can be attained by the deliberate addition of water to the H-B-O system at elevated temperatures.

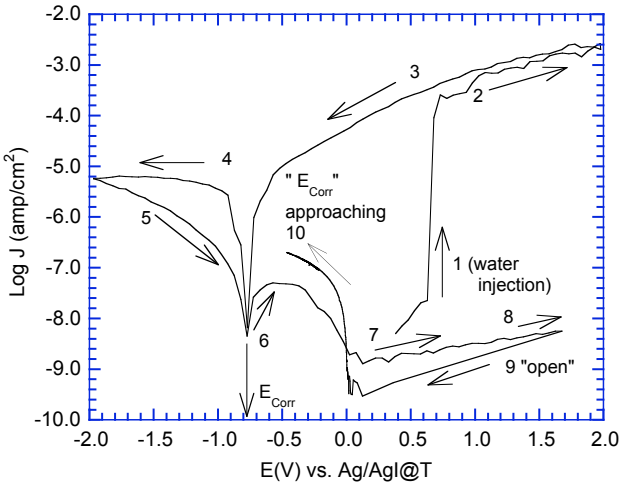

Figure 32.
Potentiodynamic test on A533 Gr.–B steel in molten HBO_2 + B_2O_3 system with addition of water.

3.1.3 Tests in High–Temperature High–Pressure Aqueous Solutions

The ECP of A533 Gr.–B steel, Alloy 600, 308 SS clad, and Pt wire in PWR water with 1000 or 9090 ppm B, ≈2 ppm Li, <10 ppb DO, and ≈2 ppm dissolved hydrogen at 25–316°C and 12.4 MPa (1800 psi) pressure are compiled in Tables 4 and 5. The change in ECP with temperature for the two water chemistries is plotted in Figs. 33a and b. In general, the ECP of all alloys decreased with an increase in temperature. At temperatures below 150°C, the ECP of A533 Gr.–B low–alloy steel is significantly lower than that of the other alloys, and at higher temperatures, the ECPs of all alloys in the two environments are comparable.

Table 4. Measured ECP (mV vs. SHE) of various alloys in water containing 9,090 ppm B, 2 ppm Li, and ≈2 ppm dissolved hydrogen at temperatures between 25 and 316°C and 12.4 MPa pressure

Temperature (°C)	A533 Gr.–B	Alloy 600	308 SS Clad	Pt
25	-0.455	0.026	0.176	0.176
100	-0.487	-0.098	-0.011	-0.040
130	-0.491	-0.152	-0.176	-0.166
150	-0.500	-0.400	-0.196	-0.210
200	-0.543	-0.487	-0.298	-0.469
288	-0.577	-0.598	-0.505	-0.606

Table 5. Measured ECP (mV vs. SHE) of various alloys in water containing 1,000 ppm B, 2 ppm Li, and ≈2 ppm dissolved hydrogen at temperatures between 150 and 316°C and 12.4 MPa pressure

Temperature (°C)	A533 Gr.–B	Alloy 600	308 SS Clad	Pt
150	-0.459	-0.504	-0.420	-0.420
200	-0.565	-0.568	-0.545	-0.567
250	-0.640	-0.638	-0.636	-0.637
288	-0.701	-0.696	-0.697	-0.693
316	-0.746	-0.740	-0.743	-0.739

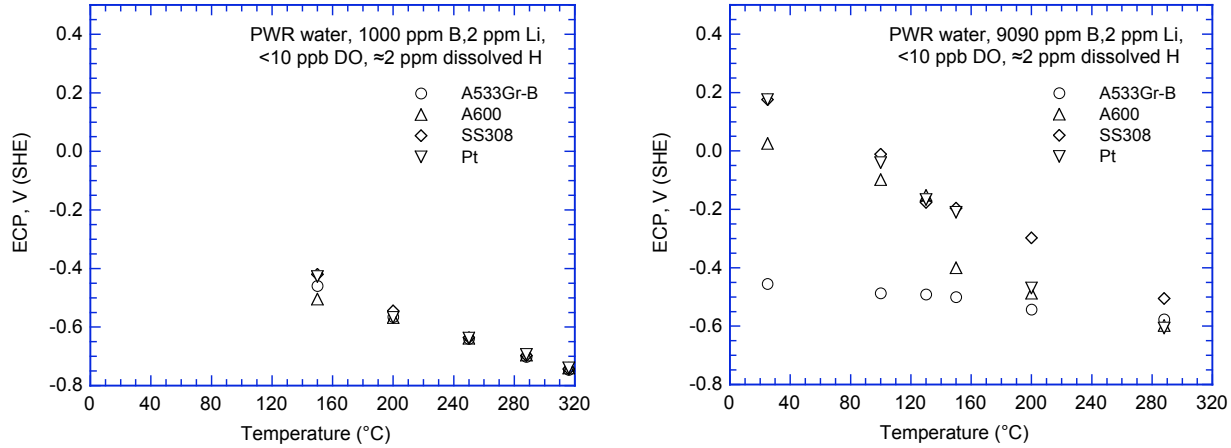

Figure 33. Change in ECP of A533 Gr.–B steel, Alloy 600, and 308 SS weld metal in water containing 1,000 or 9,090 ppm B, 2 ppm Li, and ≈ 2 ppm dissolved hydrogen at temperatures between 150 and 316°C and 12.4 MPa pressure.

3.2 Wastage Corrosion Tests

Corrosion tests were performed to measure the wastage rates of A533B pressure vessel steel, Alloy 600, and Type 308 SS cladding in the boric acid solutions of varying concentrations at 100–316°C under aerated and deaerated conditions. Corrosion tests at 97.5°C and ambient pressure were performed in saturated (37000 wppm B) and half-saturated (18500 wppm B) solutions of boric acid, simulated PWR water (1000 wppm B), and ultra high purity (UHP) water. In addition, tests were conducted in molten boric acid and boric oxide mixtures under pressure and humidity condition that provide chemical compound stability for the molten species. The corrosion tests in the temperature range between 150 and 170°C in the ambient atmosphere were conducted with and without adding water to the boric acid. Corrosion tests at 100-316°C (212–600°F) and 12.4 MPa (1800 psi) were performed in flowing room–temperature saturated boric acid solution under a hydrogen cover gas.

3.2.1 Saturated Boric Acid Solution at 97.5°C

Corrosion tests were conducted on ring specimens of A533 Gr.–B low alloy steel, Alloy 600, and Type 308 SS weld cladding, at 97.5°C in aerated solutions of boric acid that were saturated (37,000 wppm B) or half–saturated (18,500 wppm B) at the test temperature. Tests were also conducted in deaerated saturated solutions of boric acid at 97.5°C. Insulating O–rings were placed at several locations in the stack to protect against galvanic effects between

adjacent samples and/or to serve as spacers. Rubber spacers were also placed at both ends of the stack to provide protection from edge corrosion. The specimens were rotated at 50 rpm to simulate flow. Corrosion rates were determined from measurements of specimen wall thickness for time periods between 24 and 411 h. The average corrosion rates are given in Table 6 for A533 Gr.–B low-alloy steel in aerated and deaerated saturated boric acid solutions, and in Table 7 for aerated half–saturated solution of boric acid.

A significant difference in the corrosion behavior was observed between the Alloy 600 and 308 SS cladding and A533 Gr.–B specimens. The corrosion rates for Alloy 600 and Type 308 SS cladding were found to be negligible compared to those for A533 Gr.–B steel. Figure 34 shows photographs of the specimen holder immediately after 100–h exposure to aerated saturated boric acid solution at 97.5°C and after the specimens were rinsed in ultra-high-purity water. A photograph of the ring test specimens and the specimen holder after 411–h exposure to aerated saturated solution of boric acid is shown in Fig. 35, and individual specimens exposed to various specimens are shown in Fig. 36. After exposure, the A533 Gr.–B samples were covered with dark deposits, Fig. 34(a), but after rinsing they had a shiny metallic surface, Fig. 34(b). In contrast, the Type 308 clad specimens had a shiny surface and showed no corrosion.

Table. 6. Average corrosion rates for A533 Gr.–B low-alloy steel in aerated and deaerated saturated solutions* of boric acid at 97.5°C.

Corrosion Rate Measurement Times		Ave. Corrosion Rate for the Time Interval (mm/y)		
Time Interval (h)	Specimen Exposure Time (h)	Aerated Solution	Deaerated Solution	Remarks
0 – 24	24	93.1	125.2	Samples stacks were rotated at 50 rpm. Aerated condition: open to the air. Deaerated condition: purged with 1%H_2-N_2 gas.
0 – 76	76	60.5	53.4	
24 – 100	76	58.8	71.2	
0 – 100	100	67.0	84.2	
0 – 311	311	42.7	25.1	
100 – 411	311	42.3	26.4	
0 – 411	411	48.3	40.5	

*The same solutions were maintained for 411 h.

Table 7. Average corrosion rates for A533 Gr.–B low-alloy steel in aerated saturated and half-saturated solutions* of boric acid at 97.5°C.

Corrosion Rate Measurement Times		Corrosion Rate at 97.5°C (mm/yr)		
Time Interval (h)	Specimen Exposure Time (h)	Saturated BA Solution (37,000 wt. ppm B)	Half-Saturated Boric Acid Solution (18,500 wt. ppm B)	Ratio of Corrosion Rate in Saturated Solution to that in Half-Saturated Solution
0 – 24	24	93.1	40.7	2.294
0 – 76	76	60.5	24.7	2.452
24 – 100	76	58.8	28.6	2.054
0 – 100	100	67.0	31.5	2.127
0 – 311	311	42.7	16.7	2.564
100 – 411	311	42.3	20.6	2.053
0 – 411	411	48.3	23.3	2.073

*The same solutions were maintained for 411 h.

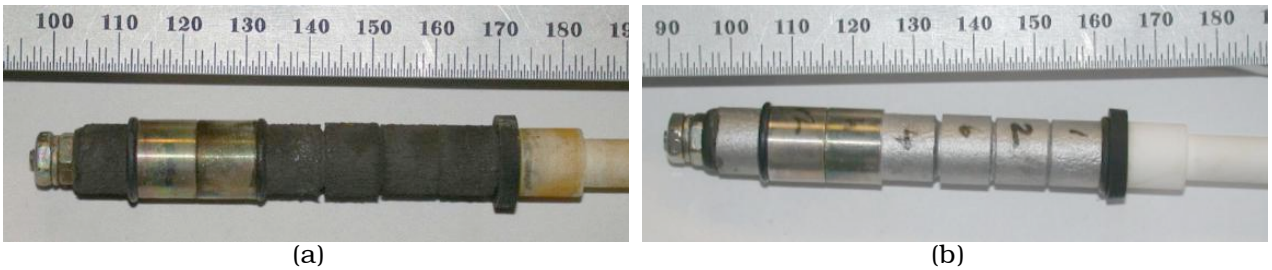

(a) (b)

Figure 34. Ring-test specimen holder (a) after 100-h exposure in aerated saturated boric acid solution at 97.5°C and (b) after rinsing in ultra high–purity water.

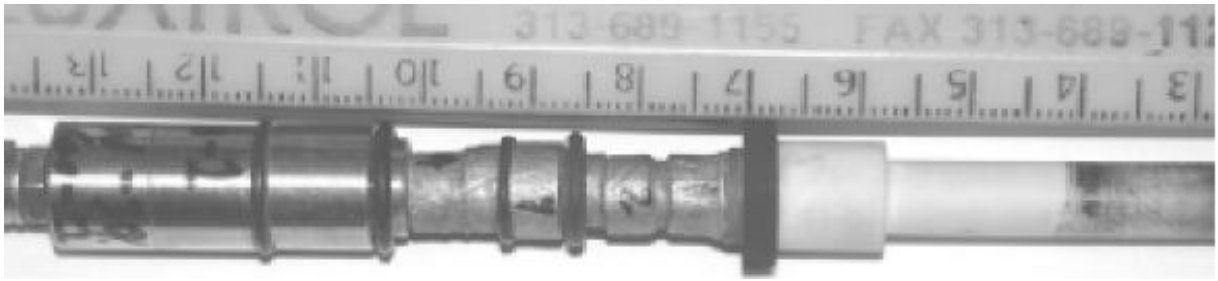

Figure 35. Ring-test specimen holder after 411–h exposure to aerated saturated boric acid solution at 97.5°C.

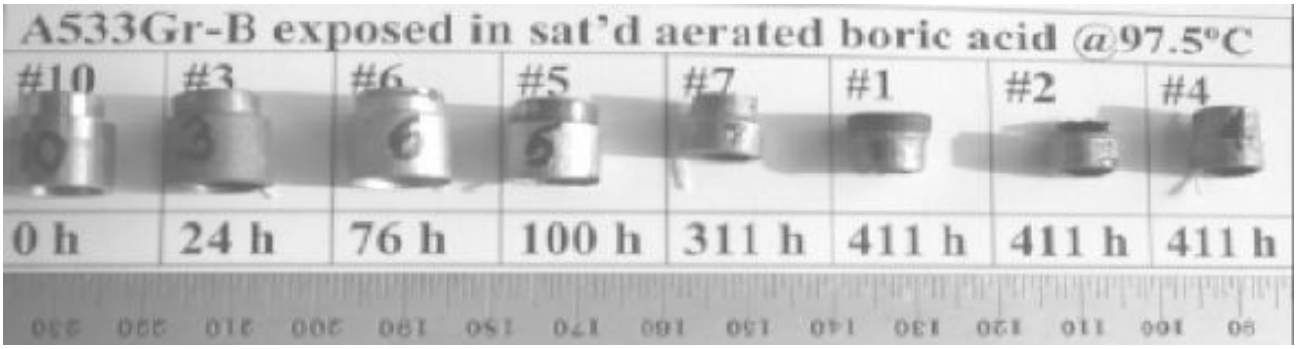

Figure 36. A533 Gr.–B specimens exposed to aerated saturated boric acid solution at 97.5°C for times up to 411 h.

The average corrosion rates of A533 Gr.–B steel in various boric acid solutions at 97.5°C are shown in Fig. 37. The rates determined from short exposure periods, e.g., 24 h, are generally higher than those determined from longer exposure periods. The corrosion rates in half–saturated solution are a factor of ≈2 lower than in saturated solution; the rates for deaerated solution are slightly lower than in aerated solution. The higher rates for short–term tests most likely are due to higher reactivity of a fresh solution. The corrosion rate from a 24–h test in deaerated half–saturated solution of boric acid that was earlier used for a 411–h corrosion test (closed symbols in Fig. 37) is comparable to the rates observed for the long–term tests.

Figure 38a shows the A533-Gr B low-alloy steel ring specimen exposed to saturated boric acid solution at 97.5°C for 311 h; the cross sectional view of the original specimen is shown in Fig. 38b. The top and bottom portions of the specimen have corroded away. Also, the overall surface morphology is similar to that observed in the large cavity observed near the Davis Besse nozzle #3. Figure 38c shows the SEM micrograph of the surface near the edge of the specimen. Figure 38d shows an SEM micrograph of the cross section of the edge of the specimen exposed for 311 h in a saturated boric acid solution at 97.5°C. A very porous part of the sample edge ≈20–μm–thick region was observed after ultrasonic cleaning using dry ethanol.

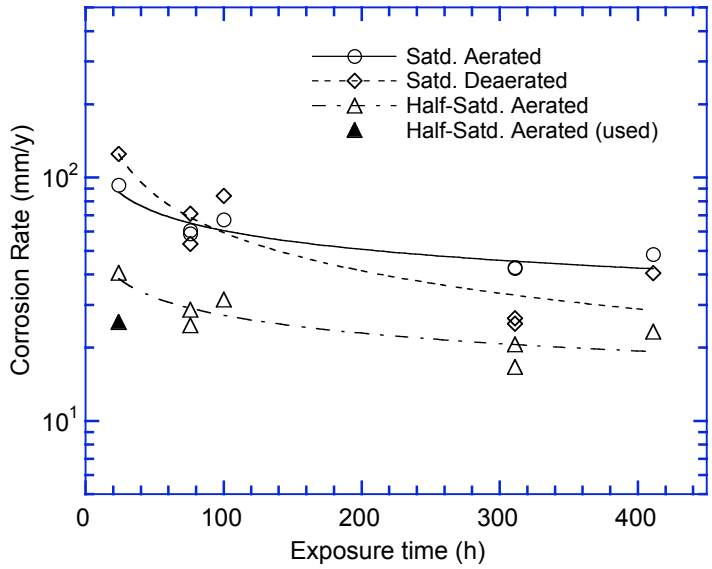

Figure 37.
Average corrosion rates for A533 Gr.–B in various boric acid solutions at 97.5°C

Figure 39 shows a schematic representation for the corrosion of low–alloy steel investigated in concentrated boric acid solution. Based on post–test examination of corrosion test specimens, we explain the most relevant evidences for the corrosion mechanism as follows:

(a) In the deaerated condition, the solution becomes pale blue but remains clear, i.e., Fe^{2+} ion dissolution. In the aerated condition, the solution becomes reddish and contains brownish-black deposit around the flask, i.e., Fe^{2+} or $Fe(OH)_3$, etc.,

(b) Gas bubbles generate and travel upward very vigorously around the A533 Gr.–B ring samples, i.e., hydrogen formation, under both aerated and deaerated conditions,

(c) Sample surface becomes dark indicating formation of a black scale, i.e., Fe_3C residue collects on the surface of the corroding samples, under both aerated and deaerated conditions.

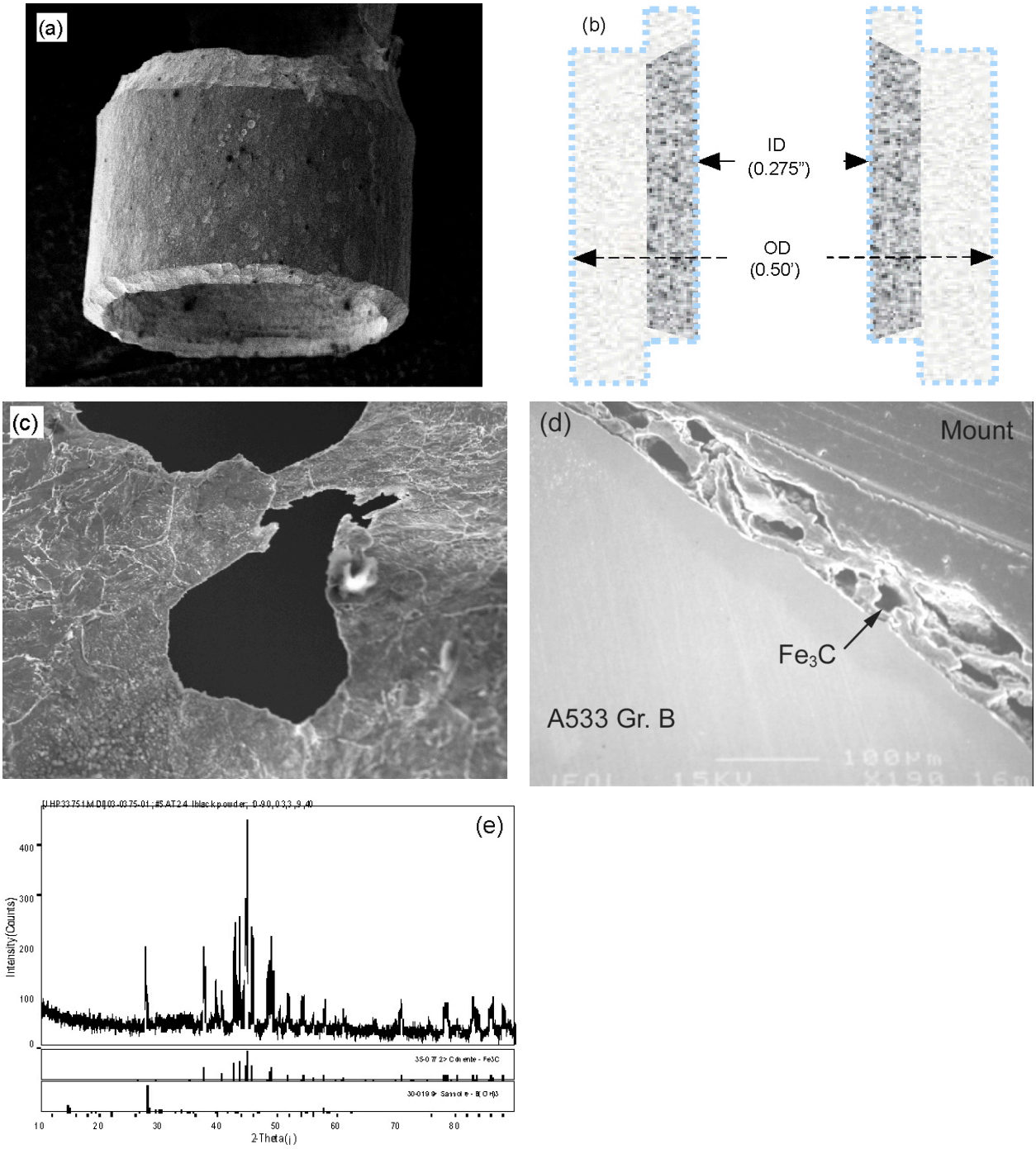

Figure 38. Geometry and metallographic evaluation of A533–Gr. B ring specimen exposed to deaerated saturated boric acid solution at 97.5°C for 411 h. (a) after ultrasonic cleaning, shape of A533–Gr. B specimen exposed for 411 h, (b) cross sectional view of the specimen as–fabricated (gray) and after the test (dark), (c) SEM micrograph of the surface of the corroded specimen in (a) at the tip of the corroding edge, (d) cross section SEM micrograph of the edge of the corroded A533–Gr. B specimen in (a) showing ≈20–mm–thick porous region with Fe_3C phase dominating the surface, and (e) x-ray diffraction analysis of the black powder identifying Fe_3C as the major phase.

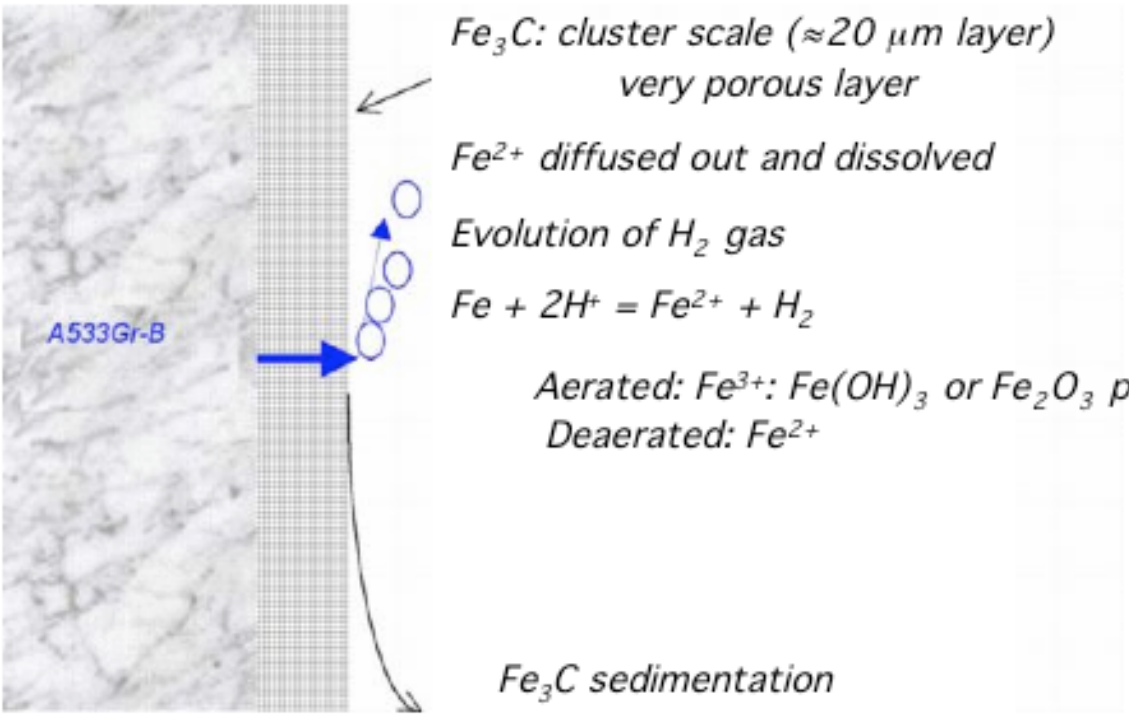

Figure 39. Schematic representation for the corrosion of low–alloy steel investigated in the concentrated boric acid solutions.

3.2.2 Molten H–B–O Environment at Ambient Pressure

Table 8 shows the corrosion data in dry H–B–O environments at 300, 260, and 150°C. The three H–B–O environments consist, respectively, of a (a) molten mixture of B_2O_3 + HBO_2 at 300°C, (b) molten HBO_2 at 260°C, and (c) a dry powder of HBO_2 + H_3BO_3 at 150°C. In the absence of moisture, no corrosion was observed for any of the materials. For corrosion to occur, the system requires a source of electron–capturing species such as protons (H^+).

Table 8. Corrosion test results in dry H–B–O environment at 300, 260, and 150°C.

Test Sample	Sample Weight (g)				Notes
	As Received	24-h test 300±9°C	26-h test 260±7°C	24-h test 154±4°C	
A533Gr-B (#9)	6.1925	6.1845	6.1832	6.1832	Little corrosion
A533Gr-B(#10)	6.2765	6.2722	6.2700	6.2700	detected
A600-2 (HT)	6.7356	6.7350	6.7342	6.7341	

Corrosion tests were also conducted in H–B–O system with additions of water. Boric acid was first heated to 260°C to obtain molten HBO_2, and water was added to the melt. The heat of evaporation cooled the system to a lower temperature, e.g., 150 and 170°C, respectively, for the two tests. The corrosion rates of A533 Gr.–B, Alloy 600, and 308 SS clad specimens in H–B–O environments at 150 and 170°C are given in Table 9.

Table 9. Test results in H–B–O system at different temperatures

Sample	As Received		150°C 45-h test		170°C 40-h test		Corrosion Rate (mm/y)	
	Wt. (g)	OD (in.)	Wt. (g)	OD (in.)	Wt. (g)	OD (in.)	150°C	170°C
A533 Gr.–B(#9)	6.1832	0.49900	3.5030	0.4530			127.94	
A533Gr.–B(#10)	6.2700	0.49900	3.9630	0.4470			144.63	
Alloy 600 CW-2	6.7341	0.49900	6.7346	0.4990			0.00	
A533 Gr.–B(#11)	6.1808	0.50000			4.9387	0.4870		36.157
A533 Gr.–B(#12)	6.1190	0.50000			5.8041	0.4942		16.132
Type 308 SS	6.7523	0.50000			6.7566	0.5000		0.00

The 308 SS and A533 Gr.–B specimens after an 40-h exposure in the H-B-O system at 170°C and ambient pressure are shown in Fig. 40a. An adherent film is seen on the 308 SS clad specimen and a non-adherent spalled scale is visible on the A533 Gr.–B specimen. Alloy 600 and A533 Gr.–B specimens tested in the H–B–O system at 150°C and ambient pressure for 45-h are shown in Figure 40b. Figure 41 shows the corrosion test results (closed diamonds) for A533 Gr.–B steel in H–B–O system with additions of water for test duration of 40–45 h. The results show significant corrosion of A533 Gr.–B steel in saturated solutions of boric acid at temperatures of 140–170°C, the corrosion rates range between ≈15–150 mm/y (0.6–6.0 in./y).

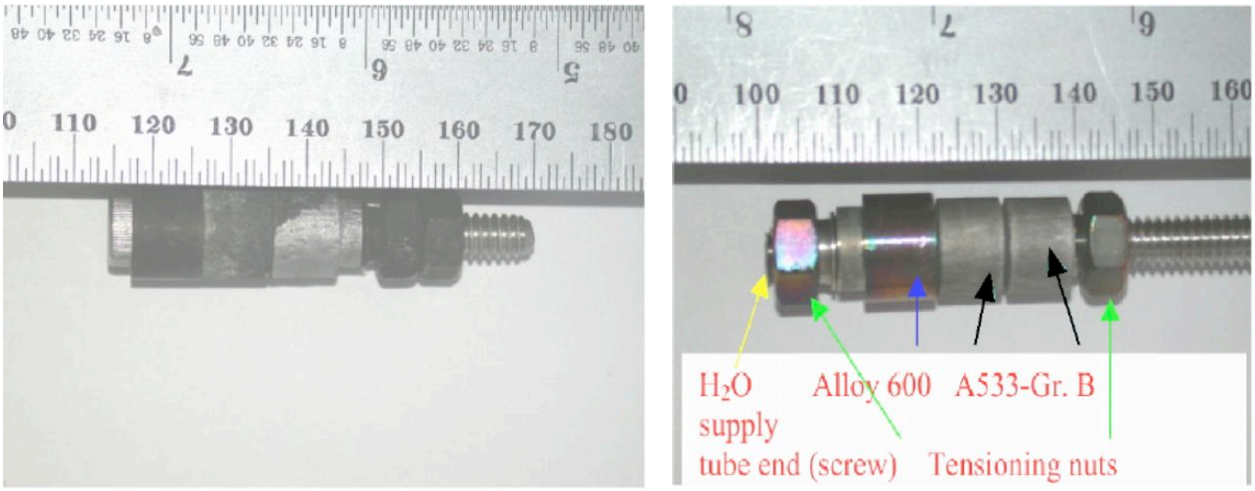

(a) (b)

Figure 40. Corrosion specimens tested in H-B-O system at 170°C and ambient pressure. (a) Type 308 SS and A533 Gr.–B specimens exposed for 40 h and (b) Alloy 600 and A533 Gr.–B specimens exposed for 45 h.

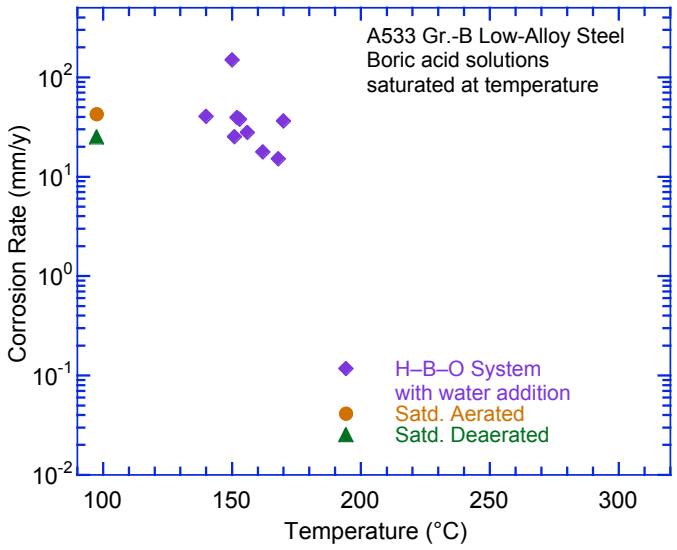

Figure 41.
Measured corrosion rates for A533 Gr.–B steel in H–B–O system with additions of water.

3.2.3 High–Temperature High–Pressure Boric Acid Solutions

Table 10 shows the observed weight changes and corrosion rates for A533 Gr.–B specimens tested at temperatures between 100 and 316°C in the room–temperature saturated boric acid (9090 wppm B). The results are plotted in Fig. 42. The results indicate that the corrosion rates for A533 Gr.–B steel are ≈4.5 mm/y at 100–150°C and decrease to ≈0.1 mm/y at 316°C. These test data show that corrosion rates of ≈5 mm/y are possible in room–temperature saturated boric acid solutions at temperatures 100–150°C and 12.4 MPa pressure. The rates fall to <1.0 mm/y at temperature ≥200°C. The implication of these results is that a wider window, from the standpoint of temperature and boric acid concentration, exits for the corrosion of low–alloy steel in a PWR system.

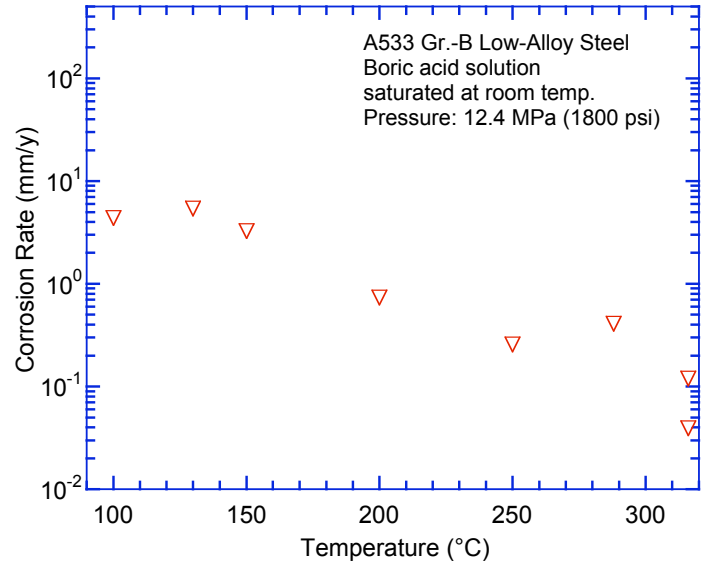

Figure 42.
Measured corrosion rates for A533 Gr.–B steel at high temperature and pressure in a room-temperature saturated boric acid solution (9090-wppm B) under hydrogen cover gas.

Table 10. Weight change data for A533-Gr. B tested at high temperature and pressure in a room-temperature-saturated boric acid solution (9090-wppm B) under hydrogen cover gas.

Temperature, Time	Sample Code	Wi (g)	Wf (g)	ΔW (g) = (Wi-Wf)	CR (mm/y)	Average CR (mm/y)
316°C, 24 h	LAS-1	0.27147	0.27128	0.00019	0.112	0.12
	LAS-2	0.26854	0.26834	0.00020	0.118	
	LAS-3	0.27466	0.27444	0.00022	0.129	
	LAS-4	0.27178	0.27158	0.00020	0.118	
316°C, 91 h	LAS-5	0.27667	0.27649	0.00018	0.0279	0.04
	LAS-6	0.27212	0.27181	0.00031	0.0481	
	LAS-7	0.26586	0.26554	0.00032	0.0497	
	LAS-8	0.27800	0.27780	0.00020	0.0310	
288°C, 24 h	LAS-9	0.27531	0.27485	0.00046	0.271	0.41
	LAS-10	0.30749	0.30668	0.00081	0.477	
	LAS-11	0.32178	0.32110	0.00068	0.400	
	LAS-12	0.24150	0.24068	0.00082	0.483	
250°C, 24 h	LAS-13	0.15433	0.15388	0.00045	0.265	0.26
	LAS-14	0.30678	0.30631	0.00047	0.277	
	LAS-15	0.27755	0.27702	0.00053	0.312	
	LAS-16	0.27583	0.27554	0.00029	0.171	
200°C, 24 h	LAS-17	0.28188	0.28105	0.00083	0.489	0.73
	LAS-18	0.28379	0.28236	0.00143	0.842	
	LAS-19	0.27710	0.27577	0.00133	0.783	
	LAS-20	0.26880	0.26741	0.00139	0.818	
150°C, 24 h	LAS-21	0.28680	0.28315	0.00365	2.148	3.25
	LAS-22	0.26527	0.25960	0.00567	3.337	
	LAS-23	0.31773	0.31307	0.00466	2.743	
	LAS-24	0.30575	0.29763	0.00812	4.779	
130°C, 24 h	LAS-25	0.25919	0.24959	0.00960	5.650	5.41
	LAS-26	0.29755	0.28793	0.00962	5.662	
	LAS-27	0.29414	0.28395	0.01019	5.997	
	LAS-28	0.30277	0.29538	0.00739	4.349	
100°C, 26 h	LAS-29	0.29876	0.29240	0.00587	3.455	4.37
	LAS-30	0.27977	0.27205	0.00713	4.194	
	LAS-31	0.32817	0.31972	0.00780	4.591	
	LAS-32	0.29065	0.28097	0.00894	5.259	

Capsule tests were also conducted on A533 Gr.–B, Alloy 600, and Type 308 SS samples to study corrosion under equilibrium conditions in the H-B-O system at high temperatures and pressures. Tests were conducted at temperatures between 170 and 316°C in a boric acid solution that was first saturated at room temperature. The temperature and pH_2O relationships for the boric acid system have been described in Section 2.2.

Weight changes for various specimens are listed in Table 11 and the visual appearance of some of the samples after testing is shown in Fig. 43. Samples exposed at 172°C showed a blossom–like deposit of hydrated iron-borate (Fig. 43a), whereas the samples exposed at higher temperatures showed only Fe_3O_4 deposits (Fig. 43b). For the A533 Gr.–B steel specimen exposed at 172°C, a very adherent layer of blossom-like deposits of iron borate was observed across the entire sample surface, resulting in a weight increase. However, even though iron oxide was deposited, all of the A533 Gr.–B disc samples lost weight. The weight changes are determined by cleaning the specimens to remove loose deposits and weighing the cleaned

Table 11. Weight and change in weight vs. temperature for the samples exposed to room-temperature saturated boric acid solution in the capsule tests for 68 h.

		A533 Gr.–B				Alloy 600			Type 308 SS		
Cell No.	Temp. (°C)	Initial Weight (g)	Final Weight (g)	Weight Change (g)	Corr. Rate (mm/y)	Initial Weight (g)	Final Weight (g)	Weight Change (g)	Initial Weight (g)	Final Weight (g)	Weight Change (g)
9	172	0.7240	0.7298	0.800[a]	–	0.3786	0.3786	0.0026	0.5690	0.5691	0.0053
10	235	0.7426	0.7421	-0.065	0.012	0.3376	0.3377	0.0180	0.5336	0.5337	0.0150
11	294	0.5950	0.5946	-0.072	0.011	0.5312	0.5312	0.0056	0.4609	0.4610	0.0087
12	316	0.5778	0.5776	-0.035	0.005	0.2905	0.2906	0.0034	0.4310	0.4311	0.0120

[a]An increase in weight because of the presence of very adherent iron borate blossom-like deposit across the entire sample surface.

specimens. The corrosion rates for A533 Gr.–B steel at 235–316°C are an order of magnitude lower than the rates observed in flowing room–temperature saturated boric acid solution (Fig. 42).

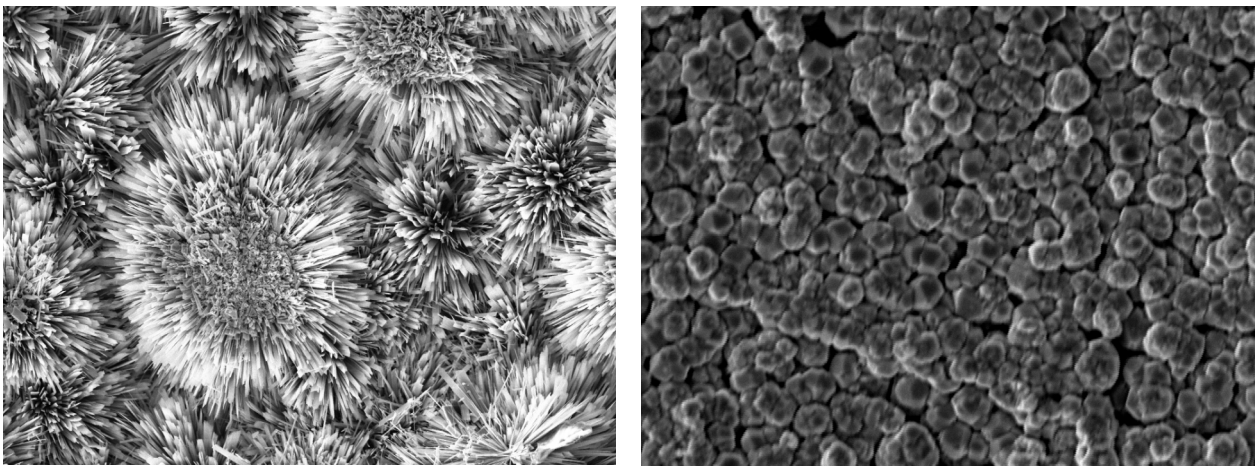

(a) (b)

Figure 43. (a) Blossom–like deposits of iron borate on A533 Gr.–B sample exposed at 172°C and (b) Fe_3O_4 deposits on the sample exposed at 294°C in room–temperature saturated boric acid solution inside a sealed capsule.

Figure 44 shows the measured corrosion rates for A533 Gr.–B steel in various boric acid solutions. As stated earlier, the corrosion process in boric acid solutions depends primarily on the physical-chemical behavior of the H-B-O system with temperature. However, the stability of $[B(OH)_4]^-$ appears to be lower at higher temperatures. This would explain the temperature dependence of the corrosion rate shown in Fig. 44 as well as the dependence on B concentration shown in Fig. 37. For a thermally activated process, corrosion rates are expected to increase with increasing temperature. For temperatures above 130°C, the temperature dependence of the corrosion rate for A533 Gr.–B steel in saturated boric acid solutions is determined by the $[H_3O]^+$ concentration; for lower temperatures, corrosion of A533 Gr.–B steel appears to be a thermally activated process. As shown earlier in Fig. 9, the pH of room-temperature saturated boric acid solution showed little temperature dependence between room temperature and 100°C, i.e., pH = 3.26; this trend continues to 150°C.

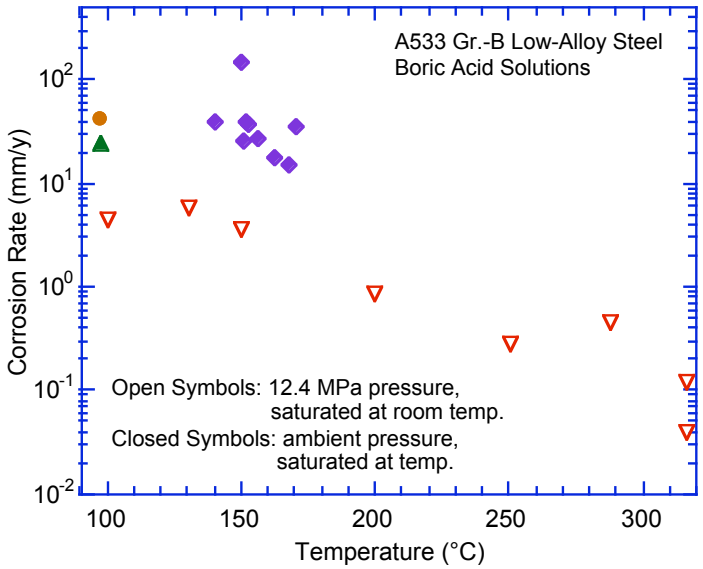

Figure 44.
Measured corrosion rates for A533 Gr.–B steel in various boric acid solutions.

Electrical conductance measurements of pure water and for aqueous boric acid solutions (containing 2,663 and 5,243 wppm B) were made over a temperature range of 25 to 350°C at the saturation vapor pressure.[11] Note that the B concentration in these solutions is below the room-temperature-saturated boric acid solution (9,090 wppm B), so all the $B(OH)_3$ would react with water to form $B(OH)_4^- + H_3O^+$ according to the reaction

$$B(OH)_3 + 2H_2O = B(OH)_4^- + H_3O^+. \quad (2)$$

The proton conductivity in solution is the highest among all the charged ions; the next highest ionic conduction species is $(OH)^-$ with a conductivity only ≈1/4 that of H_3O^+. Therefore, the electrical conductance data can provide relevant information on the proton activity in the system, and it is also useful for analysis of the data at higher temperatures i.e., T ≥100°C where a conventional pH probe could not be used. Results from this study showed a higher conductivity for the boric acid solutions than for the ultra-high-purity-water over the entire temperature range of 25 to 350°C (Fig. 45a), and increasing the boric acid concentration results in higher conductivity (Fig. 45b). All the conductivity values are higher at higher B concentrations over the entire temperature range investigated (25-350°C). However, as we see in Fig. 45c, from a plot of the slope (dσ/d[wppm B]) vs. T, we can identify three regimes of proton activity vs. boric acid concentration. At lower temperatures (T <75°C), i.e., Zone I in Fig. 45c, the conductivity increases with an increase in temperature. In Zone II (75 <T <150°C), the slope (dσ/d[wppm B]) vs. T is constant with temperature, but in Zone III (T ≥150°C), we see a negative dependence of proton conductivity on temperature.

The observed corrosion rate for the low–alloy steel seems to follow the conductivity variation with temperature. For a given boric acid or B concentration in aqueous solution, at T <100°C the corrosion rates for the low-Cr ferritic steels increase with temperature. At 100< T <150°C, the rates are fairly constant and at T >150°C, the rates decrease with an increase in temperature.

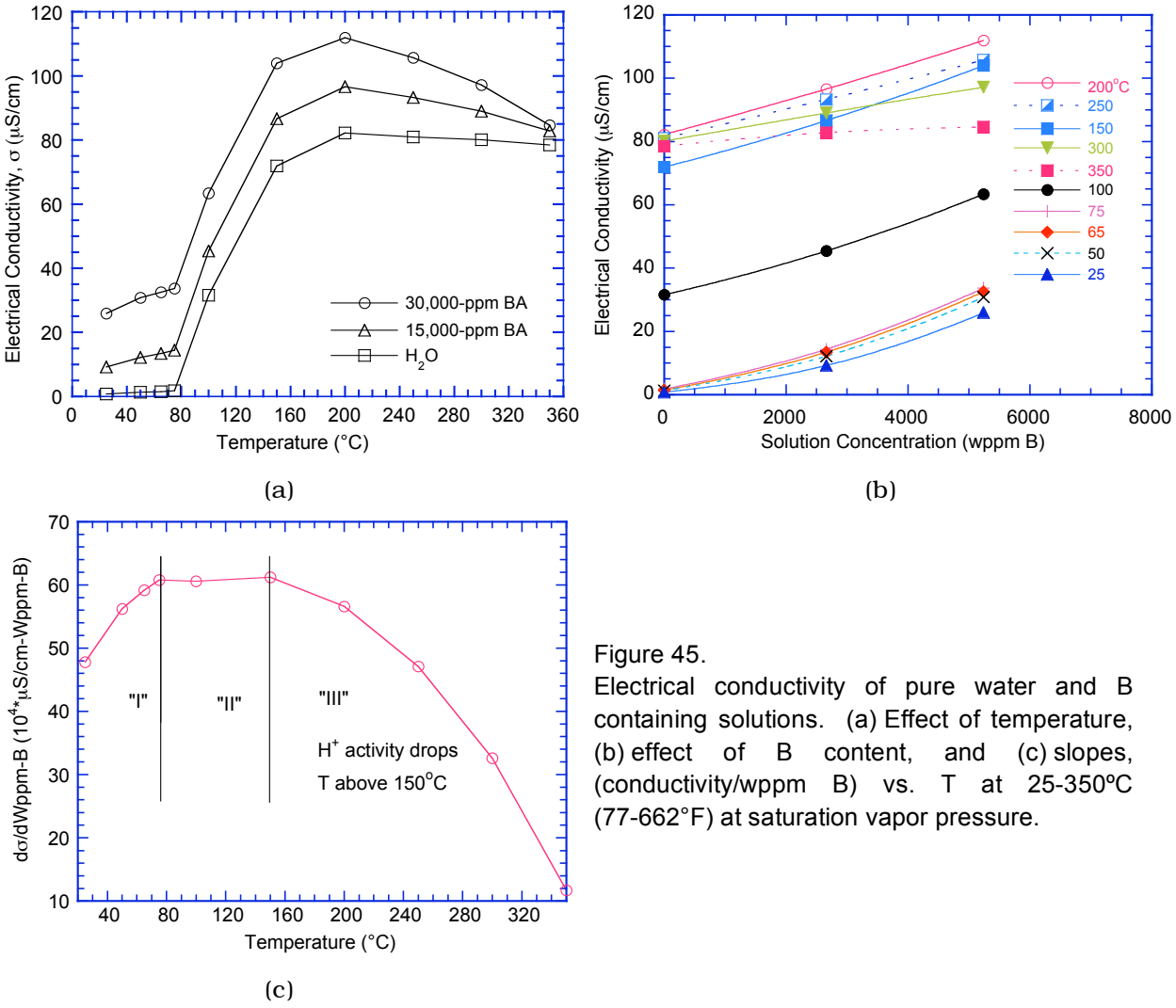

Figure 45.
Electrical conductivity of pure water and B containing solutions. (a) Effect of temperature, (b) effect of B content, and (c) slopes, (conductivity/wppm B) vs. T at 25-350ºC (77-662°F) at saturation vapor pressure.

3.2.4 Effect of Chromium Content on Corrosion Rate

It is fairly well known that the Cr content in an alloy can have a significant effect on the scale formation and corrosion performance of the alloy in aqueous environments. The effect of Cr content in the alloy on corrosion rate in aqueous environment that contains B and Li is of particular interest in PWRs, because Type 308 stainless steel weld overlay (with high Cr content) is being used on low–alloy steel reactor vessel head. To evaluate the role of Cr on the corrosion process, several alloys with varying Cr contents were exposed to room temperature saturated boric acid solution at 150, 288, and 316°C at a pressure of 12.4 MPa (1800 psig) under hydrogen cover gas. The room temperature saturated solution contained 9090 wppm B. Table 12 shows the nominal chemical compositions of the alloys used in the study. Table 13 lists the weight change data for various alloys exposed at 150, 288, and 316°C. In most cases, two specimens of each alloy were exposed.

Table. 12. Compositions of the alloys exposed in room-temperature-saturated boric acid solution.

Alloy	C	Cr	Mo	Ni	Si	Mn	Nb	V	Fe
H-1	0.096	1.0	0.47	0.08	0.09	0.001	0.002	-	Balance
H-2	0.096	2.1	0.48	0.06	0.09	0.001	0.002	-	Balance
H-3	0.094	4.5	0.46	0.06	0.13	0.005	0.005	0.002	Balance
H-6	0.098	9.5	0.50	0.07	0.01	0.002	0.005	0.001	Balance
H-9	0.094	11.9	0.49	0.05	0.01	0.001	0.010	-	Balance
308SS	0.029	21.1	0.39	9.37	0.56	1.27	-	-	Balance
Fe-25Cr	≈25 % Cr (Not analyzed in detail)								

Table 13. Weight change data for the alloys tested at high temperature and pressure in a room-temperature-saturated boric acid solution under hydrogen cover gas.

T°(C)	Wt.% Cr	Initial weight (g)	After 24-h exposure (g)	ΔW (g)	Corrosion rate (mm/y)	Average corrosion rate (mm/y)
150	0.2[1]					3.62
	1.0	0.06220	0.05720	5.0×10^{-3}	3.67	3.53
	1.0	0.05869	0.05408	4.6×10^{-3}	3.38	
	2.1	0.06312	0.05986	3.3×10^{-3}	2.39	2.14
	2.1	0.06323	0.06065	2.6×10^{-3}	1.89	
	4.5	0.06011	0.05799	2.1×10^{-3}	1.56	1.71
	4.5	0.05792	0.05539	2.5×10^{-3}	1.86	
	9.5	0.06306	0.06288	1.8×10^{-4}	0.13	0.12
	9.5	0.06305	0.06290	1.5×10^{-4}	0.10	
	11.9	0.01415	0.01411	4.0×10^{-5}	0.03	0.01
	11.9	0.01228	0.01231	-3.0×10^{-5}	-0.02	
	21.1[2]	0.46481	0.46482	-1.0×10^{-5}	-0.007	0
	21.1[2]	0.28696	0.28697	-1.0×10^{-5}	-0.007	
	25.0	0.18245	0.18243	2.0×10^{-5}	0.0147	0.02
	25.0	0.18742	0.18719	2.3×10^{-4}	0.17	
288	0.2[1]					0.45
	1.0	0.06010	0.05959	5.0×10^{-4}	0.374	0.41
	1.0	0.06357	0.06296	6.0×10^{-4}	0.448	
	2.1	0.06140	0.06084	5.6×10^{-4}	0.411	0.38
	2.1	0.06125	0.06078	4.7×10^{-4}	0.345	
	4.5	0.05798	0.05769	2.9×10^{-4}	0.213	0.20
	4.5	0.06117	0.06092	2.5×10^{-4}	0.183	
	9.5	0.06259	0.06245	1.4×10^{-4}	0.103	0.10
	9.5	0.06328	0.06315	1.3×10^{-4}	0.0954	
	11.9	0.01405	0.01399	6.0×10^{-5}	0.0440	0.07
	11.9	0.01298	0.01285	1.3×10^{-4}	0.0954	
	21.1[2]	0.44037	0.44031	6.0×10^{-5}	0.0279	0.03
	25.0	0.16327	0.16324	3.0×10^{-5}	0.0220	0.03
	25.0	0.19145	0.19140	5.0×10^{-5}	0.0367	
316	0.2[1]					0.12
	1.0	0.06433	0.06389	4.4×10^{-4}	0.323	0.30
	1.0	0.05832	0.05795	3.7×10^{-4}	0.271	
	2.1	0.06323	0.06294	2.9×10^{-4}	0.213	0.22
	2.1	0.06290	0.06260	3.0×10^{-4}	0.220	
	4.5	0.05926	0.05909	1.7×10^{-4}	0.125	0.13
	4.5	0.05734	0.05716	1.8×10^{-4}	0.132	
	9.5	0.06067	0.06058	9.0×10^{-5}	0.0660	0.06
	9.5	0.06160	0.06154	6.0×10^{-5}	0.0440	
	11.9	0.01347	0.01340	7.0×10^{-5}	0.0514	0.06
	11.9	0.01409	0.01400	9.0×10^{-5}	0.0660	
	21.1[2]	0.42574	0.42571	3.0×10^{-5}	0.0220	0.02
	25.0	0.18483	0.18483	0	0	0

[1]This row corresponds to A533 Gr.–B low alloy steel.
[2]This row corresponds to Type 308 weld metal.

Figure 46 shows a plot of average corrosion rate as a function of Cr concentration in the alloy. Also shown in the figure are the data developed on A533 Gr.–B steel (shown by open symbols) at the three temperatures. Several conclusions can be drawn from the data in Figure 46.

- The effect of increasing the Cr content of the alloy is to lower the corrosion rate at all temperatures of the study.
- At 150°C, there is a dramatic drop in corrosion rate when the Cr content of the alloy increased to 9 wt.%.
- The effect of an increase in temperature is to decrease the corrosion rate for the same boric acid concentration in the solution and for the same Cr content in the alloy.
- For a typical 308 SS weld metal with a nominal Cr content of 21 wt.%, the corrosion rate in room-temperature-saturated boric acid solution is in the range of 0.01-0.03 mm/y. The rate increases to 0.05–0.11 mm/y as the Cr content drops to 9 wt.%.

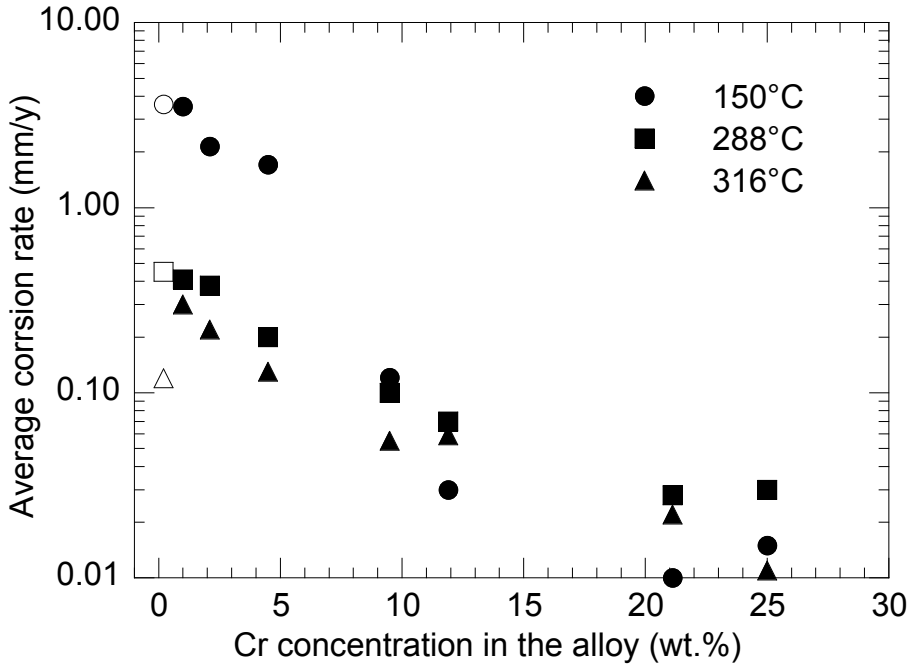

Figure 46. Effect of Cr concentration on the average corrosion rate in room-temperature-saturated boric acid solution at 150, 288, and 316°C and 12.4 MPa under H_2 cover gas.

4. Discussion

Over the years, the corrosion performance of carbon steel and low-alloy steel in boric-acid-containing aqueous environments has been studied by several investigators. Boric acid crystals have been observed at several locations in several pressurized water reactors in which the coolant contained nominally 1000 ppm B as boric acid and 2 ppm Li as lithium hydroxide. Solid boric acid crystals by themselves have been of little concern from the corrosion standpoint of ferritic steels; however, the presence of water/moisture and oxygen can lead to enhanced corrosion of ferritic steels, especially at elevated temperatures. For example, highly concentrated solutions of boric acid, albeit locally, can increase the H ion concentration (decrease the pH) in the solution and make the environment more acidic (see Figure 9c), even though boric acid by itself is considered a weak acid when compared with hydrochloric or nitric acids.

Studies have been conducted to evaluate the uniform wastage of carbon and low-alloy steels in simulated environments with emphasis on evaluation of the role of key variables such as temperature, boric acid concentration, flow velocity, specimen/crevice geometry, aeration/deaeration, etc., in corrosion.

The Electric Power Research Institute (EPRI) conducted a series of tests in which carbon and low-alloy steel specimens were buried in boric acid crystals at room temperature and exposed to water saturated flowing air for 60 days. They concluded that the average corrosion rates for the steels were 0.001-0.005 mm/y.[12]

The Moscow Power Institute conducted a series of tests by immersing plate–type carbon steel specimens in aerated and deaerated borated water for up to 1000 h. They reported long–term corrosion rates of 0.005 mm/y in aerated water with 3000 ppm B at 310°C and 0.008 mm/y in aerated water with 1000 ppm B at 200°C.[13,14]

Combustion Engineering conducted a series of tests with unclad SA-533 Grade B steels (among others) by immersing them in an autoclave with deionized, aerated water and 723 ppm B, 1.8 ppm Li, and 0.4 ppm ammonia.[15] The specimens were held at 176°C for 70 h. They reported an average corrosion rate of 0.41-0.43 mm/y. Brookhaven National Laboratory conducted tests on several carbon and low-alloy steels at 100 and 178°C in aerated water containing 4000 ppm B and LiOH at a pH of 7.3.[16] The study reported rates of 1.2-1.4 and 2.8-3.3 mm/y at 178 and 100°C, respectively.

Westinghouse performed immersion and dripping tests on low-alloy steel in aerated and deaerated boric acid solutions.[17] The test solutions were identified as 15 and 25%. The solutions were termed “aerated,” if they were left open to air during the exposure of the test specimens. The solutions were termed “deaerated,” if the system was closed and the oxygen in solution was assumed consumed by the test specimens. No direct measurements were made of the oxygen content of the solutions. The study reported corrosion rates of 122 and 76 mm/y at 93°C for low-alloy steel immersed in 25% solution in aerated and deaerated conditions, respectively. Westinghouse also reported corrosion rates in the range of 4.2–4.8 mm/y at 99°C for steel dip tested in air in a 15% solution of boric acid. Results from this study indicate that the presence of oxygen and high concentrations of boric acid in an aqueous solution can lead to very high corrosion rates for the low-alloy steel. Furthermore, the so-called “deaerated”

condition decreases the rate from 122 to 76 mm/y (≈38%). The rate still seems high indicating the possibility that the oxygen level may not be as low as one would expect under deaeration achieved by bubbling of hydrogen gas. The data also indicate that corrosion rates for the low-alloy steel are of similar magnitude, when exposed in immersion or in dip tests. Westinghouse also reported no corrosion of carbon steel specimens when exposed to dry boric acid crystals at 260°C.

Combustion Engineering also conducted immersion experiments with carbon and low-alloy steels in aerated solutions with B concentrations of 22,000 ppm and saturated value (≈40,000 ppm) at 104°C.[16,18] In these experiments they immersed plate-type specimens of SA-533 Grade B (among others) in a flask with water-cooled condensers at the top to prevent evaporation of the test solutions. Specimens were removed at various intervals to determine the corrosion progress with time and to evaluate the corrosion rates. Combustion Engineering reported corrosion rates of 16.5 and 9.1 mm/y after 24 and 96 h exposures in a solution containing 22,000 ppm B and a pH of 3.0. The rates were 36.1 and 7.6 mm/y after 6– and 27–h exposures in a solution containing 26,200 ppm B and a pH of 4.0. Combustion Engineering did not report data for low alloy steel in the B-saturated solution, but reported a corrosion rate (based on a 4-h exposure) of 184 mm/y for SA-106 Gr B carbon steel. These results indicate that the initial corrosion rates are, in general, higher than those based on long time exposures. Combustion Engineering also reported that the corrosion rate differences between different ferritic steels (SA-106, SA-533, and SA-508) were small, when tested in a given environment. The study attributed the reduction in the average corrosion rate with increasing test duration to lack of replenishing of the solution during the test, since the pH changed from 3-4 at the start of the test to 5-6 at the end of testing. The study concluded that replenishing the solutions, as is the case with many leaking joints, would have increased the corrosion rates.

Babcock and Wilcox also conducted four tests to evaluate the corrosion of carbon steel in a boric acid environment using a test apparatus that consisted of a 0.9-m-long steel pipe supported at a 30° angle from the horizontal.[19] The pipe was heated from the inside to 260-288°C, and 0.6 m of the pipe was covered by insulation that was separated from the pipe surface by a 19–mm annulus. Simulated primary water (borated and lithiated) at 93°C was then dripped onto the exposed surface of the pipe at three locations. The boric acid concentration was 13,000–14,300 ppm (2270–2500 ppm B), and the Li concentration was 1.3–1.7 ppm. The test duration ranged between 198 and 263 h. The dripped water evaporated as it was heated by the hot pipe surface, which led to an increase in boric acid concentration. At the completion of the tests, the pipes were cut and analyzed to obtain corrosion depths. The highest corrosion rates in the four tests were 102-198 mm/y and the lowest rates ranged between 0 and 7.7 mm/y. The study concluded that corrosion rates can be as high as 76–127 mm/y at downstream locations where cold borated water drips directly onto carbon steel surfaces, and that the rates can be even higher where boric acid condenses on metal surfaces near 93°C.

Recently, corrosion rate data were obtained at 100°C by Arioka* on alloys containing 4, 8, 11.5, and 15 wt.% Cr in deaerated aqueous solutions containing boric acid concentrations of

*Private communication from R. W. Staehle to W. H. Cullen (USNRC), forwarded to K. Natesan (ANL) and also from K. Arioka (Japan) to J. H. Park (ANL).

7,000, 21,000, and 38,000 ppm B. Section loss calculated from the weight change data showed corrosion rates of 6.1, 31.5, and 114 mm/y for an alloy containing 4 wt.% Cr.

Several conclusions can be drawn form the results presented above from various studies:

- Corrosion of low-alloy steel is minimal when the steel is exposed at room temperature to solid boric acid crystals even in the presence of flowing humid air (Southwest Research study)[12] or when exposed to dry boric acid crystals at 200°C (Westinghouse study).[17]
- Presence of boric acid at high concentrations in aerated aqueous solutions can increase metal wastage in ferritic steels such as carbon steel and low-alloy steels.
- Results from the BNL study[16] showed corrosion rates of 2.8-3.3 and 1.2-1.4 mm/y at 100 and 178°C, respectively, in aerated solutions with 4000 ppm B and LiOH.
- Increasing the boric acid concentration to 25% in solution (≈9,000 ppm B) resulted in corrosion rates of 122 and 76 mm/y at 93°C under aerated and deaerated conditions, respectively, (Westinghouse study).[17]
- Corrosion rates are similar for ferritic steels exposed to boric acid solutions, irrespective of whether the specimen is immersed in the solution or the boric acid solution is dripped onto the specimens.
- There is very little quantitative corrosion rate information in the temperature range of ≈100-250°C in solutions that contain a wide range of boric acid concentrations.
- There is a lack of corrosion information in molten salt type environments that are potentially feasible in H-B-O system at intermediate temperatures.
- There is a lack of corrosion information in high-pressure, high-temperature boric-acid containing environments.

The overall objective of the ANL program was to conduct research in specific areas focused to determine the conditions that can lead to aggressive and rapid rate of attack of pressure vessel steel in the presence of high concentrations of boric acid in nuclear power plants. For this purpose, the ANL study was conducted in three different and distinct environmental conditions to understand the corrosion performance of reactor steels exposed to H-B-O system.

The three environments used in the study are 1) room-temperature saturated boric acid solution in aerated and deaerated conditions for ECP and corrosion experiments at 95°C, 2) molten-salt solutions with and without water additions for corrosion tests at 150-320°C, 1 atm, and 3) high-pressure (12.4 MPa) high-temperature (up to 316°C) water with a range of boric acid solution concentrations for ECP and corrosion experiments.

- The selected environments address the following scenarios:

  Low leakage, nozzle/annulus open: water flashes, leaving boric acid deposits on RPV head surfaces at >300°C; high-temperature molten salt solutions at ambient pressure with or without moisture.

Low leakage, nozzle/annulus plugged: similar environment on both sides of the nozzle; high-temperature high-pressure PWR environment with varying boron and lithium content.

Higher leak rate (≈0.1 gal/min) & nozzle/annulus open: heat of evaporation provides cooling; low-temperature saturated boric acid solutions concentrated through boiling & enhanced by oxygen from ambient atmosphere.

- The study showed corrosion rates of 40 mm/y for A533 Gr.–B low-alloy steel at 97.5°C when tested in room-temperature saturated boric acid solution. The rates in half–saturated solution were a factor of 2 lower than in saturated solution. The rates in deaerated solutions were half as much as in aerated solutions for a given boric acid concentration.
- No corrosion was observed in any of the alloys (including A533 steel) in molten H-B-O salt when moisture was not present.
- Very high corrosion rates were observed for the A533 steel at 140-170°C in super saturated H–B–O solutions when water was added. Rates up to 150 mm/y were measured at 150°C (Figs. 47 and 48).
- The corrosion experiments in high temperature-high pressure water containing 4,000 and 9,090 wppm B showed rates of <0.1 and 8 mm/y at temperatures of 316 and 100°C, respectively (Fig. 49).

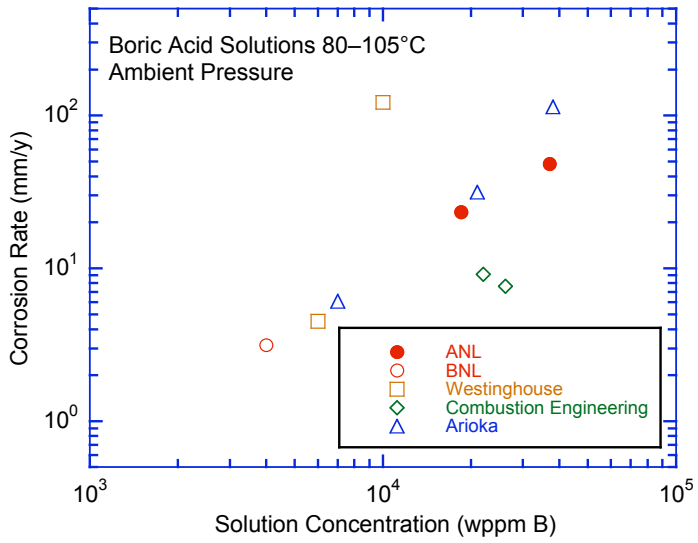

Figure 47.
Measured corrosion rates for low–alloy steels in various solutions of boric acid at 80-104°C and ambient pressure.

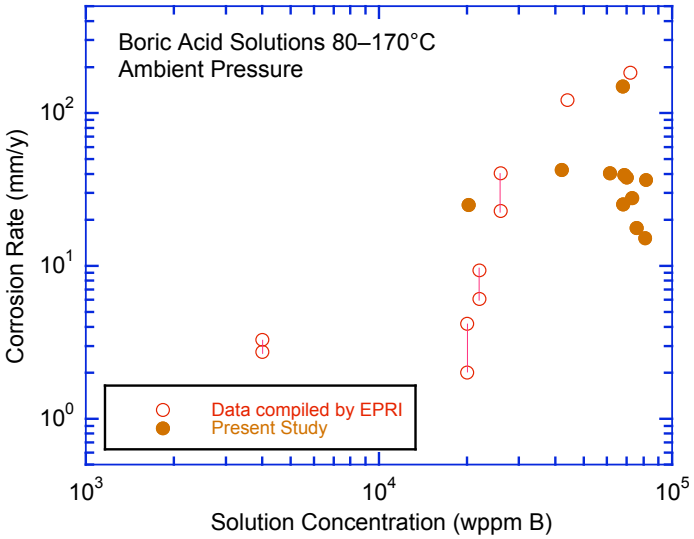

Figure 48.
Measured corrosion rates for low–alloy steels in various solutions of boric acid at 80–170°C and ambient pressure.

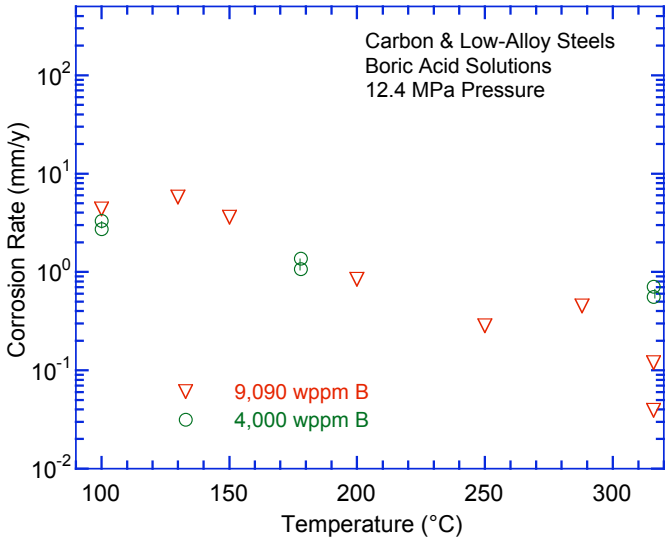

Figure 49.
Measured corrosion rates for carbon and low–alloy steels in boric acid solutions at 12.4 MPa pressure.

5. Summary

This report presents experimental data on ECP and corrosion/wastage rates for the materials found in the RPV head and nozzles of a typical PWR in boric acid solutions of varying concentrations at temperatures of 95–316°C (203–600°F). Tests were conducted in environmental conditions that have been postulated in the CRDM nozzle/head crevice: (a) high–temperature, high–pressure aqueous environment with a range of boric acid solution concentrations; (b) high-temperature (150–300°C) boric acid powder at atmospheric pressure with and without the addition of water; and (c) low–temperature (≈95°C) saturated boric acid solutions both deaerated and aerated. These environmental conditions correspond to the following situations: (a) low leakage through nozzle crack and nozzle/annulus plugged, (b) low leakage through nozzle crack and nozzle/annulus open, and (c) significant cooling due to high leakage through nozzle crack and nozzle/annulus open.

Test facilities were assembled to perform ECP and corrosion rate measurements on A533 Gr.–B low–alloy steel, Alloy 600, and 308 SS weld clad, in the various postulated environments in the CRDM nozzle/head crevice. In general, the ECP of all alloys decreased with an increase in temperature. At temperatures below 150°C the ECP of A533 Gr.–B low–alloy steel was significantly lower than that of the other alloys. Also, at 95°C, the ECP of A533 Gr.–B steel decreased slightly as the concentration of boric acid in the solution was decreased from 36,000 ppm to 3,500 ppm. At 150–316°C and 12.4 MPa (1800 psi) pressure, the ECP of all alloys were comparable in PWR water with 1000 or 9090 ppm B, ≈2 ppm Li, <10 ppb DO, and ≈2 ppm dissolved hydrogen.

In the various environments investigated in the present study, the corrosion rates of Alloy 600 and 308 SS cladding were found to be negligible compared to those of A533 Gr.–B steel. Also, in the absence of moisture, no corrosion was observed for any of the materials in H–B–O environments at 150, 260, and 300°C; the H–B–O environments consist of a dry powder of HBO_2 + H_3BO_3 at 150°C, molten HBO_2 at 260°C, and molten mixture of HBO_2 + B_2O_3 at 300°C.

For A533 Gr.–B steel, an average corrosion rate of ≈40 mm/y (1.6 in./y) was measured in aerated saturated solution of boric acid at 97.5°C and ambient pressure. The corrosion rate in aerated half–saturated solution was a factor of ≈2 lower than in saturated solution; the rates for deaerated solution were ≈40% lower than in aerated solution. Very high corrosion rates were observed for A533 Gr.–B steel at 140–170°C in super–saturated molten salt solutions of boric acid with addition of water. Short-term corrosion rates up to 150 mm/y were measured at 150°C.

The corrosion experiments in high–temperature high–pressure water containing 9090 ppm B, ≈2 ppm Li, <10 ppb DO, and ≈2 ppm dissolved hydrogen showed that the corrosion rates decreased with increasing temperature. The rates were ≈5 mm/y at 100–150°C and decreased to <0.1 mm/y at 316°C.

The existing corrosion/wastage data in boric acid solutions in the literature have been summarized. The earlier studies, predominantly conducted at 80–104°C, showed that the corrosion rates for low–alloy steel can increase from ≈3 mm/y to greater than 100 mm/y as the B concentration in the solution was increased from ≈4,000 to 40,000 wppm. The results from

the present study in saturated boric acid solutions at 97.5°C are in agreement with the earlier data. In addition, very high corrosion rates were observed for low–alloy steel at 140–170°C in molten salt solutions of boric acid with addition of water. Short-term corrosion rates up to 150 mm/y were measured at 150°C, which are in the same range that was observed in saturated boric acid solutions at 97.5°C. The corrosion rate data developed over a wide temperature range in the present study may be used to assess the corrosion performance of the RPV and CRDM nozzle materials in boric acid solutions.

References

1. Nuclear Regulatory Commission (U.S.), Bulletin 2001–01, "Circumferential Cracking of Reactor Pressure Vessel Head Penetration Nozzles," Aug. 3, 2001.

2. Nuclear Regulatory Commission (U.S.), Information Notice 2002–11, "Recent Experience with Degradation of Reactor Pressure Vessel Head," March 12, 2002.

3. Loehlein, S., et. al., "Root Cause Analysis Report: Significant Degradation of the Reactor Pressure Vessel Head," CR 2002≈0891, First Energy, Davis–Besse Nuclear Power Station, April 15, 2002.

4. U.S. Nuclear Regulatory Commission, Information Notice 2001–05, "Through–Wall Circumferential Cracking of Reactor Pressure Vessel Head Control Rod Drive Mechanism Penetration Nozzles at Oconee Nuclear Station, Unit 3," April 30, 2001.

5. Hunt, E. S., "Boric Acid Corrosion Guidebook, Revision 1: Managing Boric Acid Corrosion Issues at PWR Power Stations," Final Report 1000975, EPRI, Palo Alto, CA, Nov. 2001.

6. Latimer, W. H. and H. Hildebrand, *Reference Book of Inorganic Chemistry*, MacMillan, NY, 1951.

7. Linke, W. F., *Solubilities, Inorganic and Metal–Organic Compounds*, Vol. I and II, Fourth Edition, American Chemical Society, Washington, DC, 1965.

8. Knacke, O., O. Kubaschewski,, and K. Hesselmann, *Thermochemical Properties of Inorganic Substance*, Springer-Verlag, 2nd ed., 1991.

9. ASTM Designation G5–94, "Standard Reference Test Method for Making Potentiostatic and Potentiodynamic Anodic Polarization Measurements, Metals Test Methods and Analytical Procedures," 1999 Annual Book of ASTM Standards, Volume 03.02 Wear and Erosion; Metal Corrosion, ASTM, PA, 1999.

10. Skoog, D. A. and D. M. West, *Principles of Instrumental Analysis*, Holt, Rinehart and Winston, Inc, New York (1971).

11. Ho, P. C. and D. A. Palmer, "Electrical Conductivity Measurements of Aqueous Boric Acid at 25-350°C at Saturation Vapor Pressure," ORNL/TM-13185, Oak Ridge National Laboratory, 1995.

12. Boric Acid Corrosion Evaluation Program – Phase II Corrosion Testing, Topical Report, Southwest Research Institute, 1998.

13. Margulova, T. K., L. M. Bursuk, S. V. Bogatyreva, and A. A. Lipanina, "Corrosion of Structural Materials in the Boron-Containing Solutions Used for Controlling the Power of Nuclear Reactors," Therm. Eng., Moscow Power Institute, 1970, pp. 13-17.

14. Babei, Y. I., et al., "Influence of Boric Acid Regulation of a Medium on Carbon and Low-Cycle Corrosion Fatigue Resistance of Constructional Steels," Soviet Materials Science, pp. 135-139, 1982.

15. Hall, J. F., et al., "Boric Acid Corrosion of Carbon and Low-Alloy Steels," Proc. Fourth Intl. Symp. On Environmental Degradation of Materials in Nuclear Power Systems-Water Reactors, Jekyll Island, GA., August 6-10, pp. 9-38 to 9-52, 1989.

16. Nuclear Regulatory Commission (U.S.) (NRC), NUREG/CR-2827, "Boric Acid Corrosion of Ferritic Reactor Components," NRC, Washington, D.C., July 1982.

17. Degradation of Reactor Coolant System Pressure Boundary Resulting from Boric Acid Corrosion, Westinghouse letter NS-NRC-87-3260 to the NRC, dated October 15, 1987.

18. O'Neill, A. S. and J. F. Hall, "Boric Acid Corrosion of Carbon and Low-Alloy Steels Pressure-Boundary Components," EPRI NP-5985, Electric Power Research Institute, Palo Alto, CA, August 1988.

19. Ouellette, C. E., "B&W Boric Acid Corrosion Research and the Wastage and Inspection Procedures for RCS Leakage," BAW-2126, B&W Nuclear Sevice Company, Lynchburg, VA, December 1990.

NRC FORM 335
(9-2004)
NRCMD 3.7

U. S. NUCLEAR REGULATORY COMMISSION

BIBLIOGRAPHIC DATA SHEET

(See instructions on the reverse)

1. REPORT NUMBER
(Assigned by NRC. Add Vol., Supp., Rev., and Addendum Numbers, if any.)

NUREG/CR–6875
ANL–04/08

2. TITLE AND SUBTITLE

Boric Acid Corrosion of Light Water Reactor Pressure Vessel Head Materials

3. DATE REPORT PUBLISHED

MONTH	YEAR
July	2005

4. FIN OR GRANT NUMBER

Y6722

5. AUTHOR(S)

J. -H. Park, O. K. Chopra, K. Natesan, and W. J. Shack

6. TYPE OF REPORT

Technical

7. PERIOD COVERED (Inclusive Dates)

8. PERFORMING ORGANIZATION – NAME AND ADDRESS *(If NRC, provide Division, Office or Region, U.S. Nuclear Regulatory Commission, and mailing address; if contractor, provide name and mailing address.)*

Argonne National Laboratory
9700 South Cass Avenue
Argonne, IL 60439

9. SPONSORING ORGANIZATION – NAME AND ADDRESS *(If NRC, type "Same as above": if contractor, provide NRC Division, Office or Region, U.S. Nuclear Regulatory Commission, and mailing address.)*

Division of Engineering Technology
Office of Nuclear Regulatory Research
U.S. Nuclear Regulatory Commission
Washington, DC 20555–0001

10. SUPPLEMENTARY NOTES

William H. Cullen, Jr., NRC Project Manager

11. ABSTRACT (200 words or less)

This report presents experimental data on electrochemical potential and corrosion rates of the materials found in the reactor pressure vessel head and control rod drive mechanism (CRDM) nozzles in boric acid solutions of varying concentrations at temperatures of 95–316°C (203–600°F). Tests were conducted in postulated environmental conditions in the nozzle/head crevice, e.g., (a) high–temperature, high–pressure aqueous environment with a range of boric acid solution concentrations, (b) high-temperature (235–320°C) molten salt solutions, and (c) low–temperature (≈95°C) saturated boric acid solutions. These correspond to the following situations: (a) low leakage through the nozzle and nozzle/head annulus plugged, (b) low leakage through the nozzle and nozzle/head annulus open, and (c) significant cooling due to high leakage and nozzle/head annulus open. The results indicate significant corrosion only for the low–alloy steel and no corrosion for Alloy 600 or 308 stainless steel cladding. Also, corrosion rates were significant in saturated boric acid solutions, and no material loss was observed in boric acid melts or deposits in the absence of moisture. The results are compared with the existing corrosion/wastage data in the literature.

12. KEY WORDS/DESCRIPTORS *(List words or phrases that will assist researchers in locating this report.)*

Boric acid corrosion
Control Rod Drive Mechanism (CRDM) nozzle
Reactor pressure vessel head
High–pressure aqueous environment
Molten salt solutions
Electrochemical potential (ECP)
Corrosion rates

13. AVAILABILITY STATEMENT

unlimited

14. SECURITY CLASSIFICATION

(This Page)

unclassified

(This Report)

unclassified

15. NUMBER OF PAGES

16.PRICE

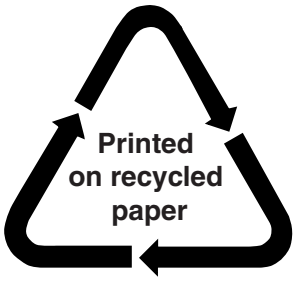

Federal Recycling Program